MODELING AND SIMULATION FOR PARTICULATE HEAT EXCHANGER

A Thesis
Presented to
The Academic Faculty

by

Lu Shen

In Partial Fulfillment
of the Requirements for the Degree
Master of Science in the
George W. Woodruff School of Mechanical Engineering

Georgia Institute of Technology
May 2017

MODELING AND SIMULATION FOR PARTICULATE HEAT EXCHANGER

Approved by:

Dr. Sheldon Jeter, Advisor
School of Mechanical Engineering
Georgia Institute of Technology

Dr. Said Abdel-Khalik
School of Mechanical Engineering
Georgia Institute of Technology

Dr. Peter Loutzenhiser
School of Mechanical Engineering
Georgia Institute of Technology

Date Approved: 04/10/2017

ACKNOWLEDGEMENTS

I would like to praise God for leading me through this thesis. His Words and wisdom have been guiding me and encouraging me. I am truly grateful for His gifts and grace.

I would like to thank my husband, Yao Tang, for being supportive, loving and caring. He always encourages me when I am in the valley, and reminds me to be humble when I am at the hilltop.

I would like to thank Dr. Sheldon Jeter for being my advisor. He is brilliant and passionate about research, setting a professinal example for me. I especially thank him for being patient and inspiring with my thesis, and he has provied constructive advise and remarkable knowledge on my theis topic. In addition, I would like to thank Dr. Said Abdel-Khalik and Dr. Peter Loutzenhiser for being my committee mumbers and proving me guidances through my thesis.

I would like to thank my parents for providing me the oppurtunity to study at Georgia Tech. Without their support and encougement, I would not have had the accomplishment this day.

Finally, I would also like to thank my research group members, Matthew Golob, Clayton Nguyen, Kenzo Repole, Ramy Imam, and Christopher Fernandez. They have dedicated their time to help me with this thesis and helped me with technical knowledge. I would also like to thank all my friends who have encourged me here at Georgia Tech, and made my experience here at Geogia Tech so special and unforgettable.

TABLE OF CONTENTS

LIST OF TABLES

LIST OF FIGURES

LIST OF SYMBOLS

Re	Reynold's number
Nu	Nusselt number
ρ	density
D_H	Hydraulic diameter
U	Velocity
μ	Dynamic viscosity
h	Heat transfer coefficient
k	Thermal conductivity
$\dot{q}$	Heat flux
T	Temperature
$\dot{m}$	Mass flow rate
Cp	Heat capacity
$\dot{Q}$	Heat transfer rate
$\dot{H}$	Enthalpy flow
ϵ	Error
L_h	Hydrodynamic entry length
$U_{overall}$	Overall heat transfer coefficient
α	Volume fraction
d_s	Particle diameter
x	Distance to wall
A	Heat transfer surface area
R	Row index

C Column index

LIST ABBREVIATIONS

AFS	Arizona Fracking Sand
ATL	Atlanta Industrial Sand
CFB	Circulating fluidized bed
CFD	Computational fluid dynamics
CSP	Concentrator Solar Power
FB	Fluidized bed
FCC	Face centered cubic
FT	Finned-tube
ID50	50 mesh intermediate density proppant
HPF	Hypothetical particulate flow
HX	Heat exchanger
MOFCG	Multiple orifice flow control grate
PFHX	Particle-fluid heat exchanger
PP	Pillow-plate

RWS	Riyadh White Sand
sCO2	Supercritical carbon dioxide
SFT	Serpentine finned-tube
UHF	Uniform heat flux
UWT	Uniform wall temperature
ZZ	Zig-zag

SUMMARY

Particle heating systems are promising candidates for Concentrator Solar Power, as they not only are suitable for very high temperature heat source for various thermal power cycles but can also store thermal energy in the particles at a low cost. However, particle to fluid heat exchangers, especially for the needed high temperatures, are an underdeveloped technology. To advance this technology, this thesis was conducted to develop an equivalent Computational Fluid Dynamics (CFD) model to represent the flow and heat transfer processes in a moving packed bed heat exchanger. In a packed bed, the particles are always in mutual contact at near the maximum packing density. While other particle flows are possible in such exchangers such as (1) moving fluidized particle beds or (2) particles flowing rapidly at moderate density with a free surface, or other flows, only moving packed bed exchangers are currently in active deployment. From past experience [1] it is known that in a moving packed bed of particles, the velocity in the bed should be nearly uniform away from the solid walls with little mixing, and the velocity gradient is expected to be small except very near solid surfaces. In fact, the solid particles will slip at the solid walls in contrast to the no-slip condition in typical fluid flows. This characteristic flow is usually referred to as a "plug flow' in heat transfer analysis for low viscosity fluids such as liquid metals. Therefore, a hypothetical fluid with either zero viscosity or a very low viscosity should simulate the particulate plug flow well enough to allow a reasonable approximation to the actual heat transfer processes. Such a continuum simulation should be very computationally efficient in comparison with any realistic but enormously complicated discrete particle simulation. Two approaches using this hypothetical particulate fluid (HPF)

are possible: developing laminar HPF flow with negligible fluid viscosity and rigorous inviscid Euler flow with zero viscosity. It was found that a widely used standard laminar flow model [2] was unstable with viscosity small enough to simulate a plug flow for the conditions necessary in this thesis. Furthermore, a rigorous inviscid Euler flow model was not provided in the available CFD package [2]. Fortunately, the commonly-available CDF package does include an "Euler-Euler" model for two phase flows. In this context "Euler-Euler" applies in the mathematical sense meaning that both phases are modeled as continuum flows in contract with a "Euler-Lagrangian" formulation in which a continuous phase is combined with a discrete phase modeled by Lagrangian particle dynamics to model the motion of the discrete elements. Numerical experimentation demonstrated that the continuous phase in the "Euler-Euler" package could be specified as having a vanishing viscosity (*i.e.* 10^{-20} Pa-s) giving an essentially inviscid Euler flow result. Ultimately it was found that only the approximate inviscid Euler flow model successfully modeled a plug flow. Presumably the latter model is for some reason more numerically robust than is commonly needed for CFD. These assumptions allow a relatively simple CFD model to represent the heat transfer characteristics of the particle flow.

At present, it is near universal practice to test the flow performance of the particulate empirically, since it is very difficult to model the flow from first principles alone. In consequence, it is of great practical utility to model the heat transfer properties of a packed bed moving at an assumed and presumably empirically verified superficial or upstream velocity. For these conditions, only the heat capacity, bulk density, and bulk thermal conductivity of the particle bed need to be known.

Ultimately two particulates were studied Riyadh White Sand (RWS) and industrial silica sand representative of silica sands available in a region with good potential for CSP and ID50 an alumina based foundry product representative of alumina based particulates that might be especially suitable for CSP applications. More details about the measurements of particle thermal conductivity are presented in Section 2.5.

The CFD model was first verified by comparison with classic simple cases of a fluid between parallel plates. The parallel-plates geometry was initially tested with a simple fluid (air) with constant material properties, for both laminar flow and Euler flow with vanishing viscosity. The simulated heat transfer coefficient and Nusselt number were almost equal to the theoretical values for both approaches. Then a HPF representing ID50 with a viscosity of 10^{-10} Pa-s is modeled with Euler flow. The heat transfer coefficient and Nusselt number were then calculated from the simulations. Comparing to the well-known theoretical results, the Euler flow results are in good agreement.

Another model was then also designed to represent an available experimental heat exchanger geometry with electric cartridge heaters supplying a constant heat flux instead of parallel plates with constant heat flux [1]. Both the laminar flow and Euler flow for HPF using RWS were simulated. The simulation results for a low viscosity laminar flow suggest a non-uniform velocity profile across the geometry, which did not represent the inviscid property of particulate flow. On the other hand, nearly–inviscid Euler flow yielded the expected results and agreed well with the experimental results. After this adjustment, the Euler-Euler was chosen for the further modeling of particulate heat transfer. Development of a rigorous inviscid Euler model was not feasible within the scope of this thesis; however, it is a topic for future work.

Therefore, the practical particulate heat transfer is modeled with Euler-Euler laminar flow numerical module with HPF representing ID50. Other details such as geometry offset and near-wall thermal resistance is added to the model. The simulation results highly agree with the results from other source [3], indicating the model has successfully represent the particle flow in both fluid dynamic and heat transfer performance.

In addition, a MATLAB script using basic principles of heat transfer is written to model the generally counter flow particulate heat exchanger with multiple tube passes. This geometry is similar to several proposed particle to fluid heat exchangers. This code not only model the temperature of the HPF, but also the temperature of the cooling fluid. This theoretical approach provided a fast and fundamental modeling of a particulate heat exchanger.

CHAPTER 1. INTRODUCTION

1.1 Particulate Heat Exchanger

Particle heating systems are promising candidates for Concentrator Solar Power (CSP), as they not only are suitable for very high temperature heat source for various thermal power cycles but can also store thermal energy in the particles at a low cost. However, particle to fluid heat exchangers, especially for the needed high temperatures, are an underdeveloped technology.

To help advance this technology, this thesis was conducted to develop an equivalent CFD model to represent the flow and heat transfer processes in a moving packed bed heat exchanger. In a moving packed bed of particles, the velocity in the bed should be nearly uniform with little mixing, and the velocity gradient is expected to be small except very near solid surfaces. Mixing is especially impeded in a moving packed bed since the particulate flow must expand to achieve any appreciable shearing. Therefore, a hypothetical fluid with sufficiently low viscosity should simulate the particulate flow well enough to allow a reasonable approximation to the actual heat transfer processes. Such a continuum simulation should be very computationally efficient in comparison with any realistic but enormously complicated discrete particle simulation.

Since For heat exchanger modeling, the heat transfer in the fluid (or HPF) is more important than the particle dynamics if the flow can be realistically simplified as in this case. Therefore, the particle-to-particle dynamics will be ignored in the particulate flow by using bulk properties of the moving bed; yet the heat transfer and dynamics between wall

and particles can still be investigated. Two approaches using this hypothetical particulate fluid (HPF) are possible: (1) developing laminar HPF flow with negligible fluid viscosity and (2) Euler-Euler flow with only continuous phase and diminishing viscosity.

1.2 COMSOL Modeling

Two approaches using this HPF for heat transfer are possible: developing laminar HPF flow with negligible fluid viscosity and approximately inviscid Euler-Euler laminar flow with near-zero viscosity. To decide on which module is more suitable for the particulate moving bed, the CFD model will be first verified by comparison with classic simple cases of a fluid between parallel plates. Then the moving packed bed represented by the HPF will be simulated with constant density equal to the measured bulk density of the particulate no comma and the measured heat capacity. The thermal conductivity is initially estimated to be the conductivity measured with a commercial transient heated probe device, which should approximate the actual conductivity of the bulk particulate. The heat transfer coefficient and Nusselt number will be then calculated from the simulations to evaluate the modeling performance.

The geometry will be then also altered to represent an available experimental heat exchanger geometry with electric cartridge heaters supplying a constant heat flux instead of parallel plates with constant heat flux. Again, both the laminar flow and Euler flow for HPF will be simulated. After this adjustment, the two module approaches will be evaluated and the more suitable one will be used in further modeling of the particulate heat transfer with much improved confidence.

1.2.1 Laminar Flow Module

Laminar flow module in COMSOL simulates a single-phase fluid in the laminar flow regime. In a laminar flow, there is no mixing, which is important for modeling moving packed beds. Physically, a flow will remain laminar as long as the Reynolds number is below a certain critical value. At higher Reynolds numbers, disturbances have a tendency to grow and cause transition to turbulence. This critical Reynolds number (Re) depends on the model, but a classical example is pipe flow where the critical Reynolds number is known to be approximately 2000. The equations solved by the Laminar Flow interface are the Navier-Stokes equations for conservation of momentum and the continuity equation for conservation of mass. Even though flow velocity in a particulate heat exchanger is about 0.01 m/s, the Reynolds Number will be very high if the viscosity is very low, so physical laminar flow of a fluid is not consistent with low viscosity. Nevertheless, as demonstrated in this thesis a laminar flow can still be computed numerically so long as the viscosity is just slightly above zero. The resulting very high Reynolds number situation would surely be unstable in practice and even leads to numerical difficulties in numerical modeling. Nevertheless, a hypothetical very low viscosity fluid is a good approximation to a moving packed bed for computational heat transfer purposes.

1.2.2 Euler-Euler Laminar Flow Module

The Euler-Euler flow module is widely used in fluidized beds and sedimentation. The module used two sets of Navier-Stokes equations for continuous phase and dispersed phase separately. The module interface is based on averaging the for each phase over a volume that is small compared to the computational domain but large compared to the dispersed phase particles, droplets, or bubbles [4]. For simplification, only continuous

phase is used because the particulate flow is simplified as one homogenous flow. Note that this “Euler-Euler” model is still intrinsically laminar, but fortunately it was found to be numerically flexible or robust enough to yield convergent solutions even for very low viscosity flows.

1.3 MATLAB Modeling

The HPF model developed in this thesis could be used in a detailed CFD model for a heat exchangers with passages for the particulate and tubes or passages for the fluid side. However, such a model is known to be highly consumptive of user time to develop and mesh the geometry and highly consumptive of computer run time. A more practical systems approach to model the heat transfer in the particulate heat exchanger is developed using principles of heat transfer in 2-D. Thus, a MATLAB script is coded to model both the hypothetical fluid and cooling fluid. The code has been completed and tested and is ready for practical applications; however, these applications are mostly for proprietary designs outside the scope of this thesis. With this model a practical heat exchanger can be modeled using heat transfer coefficients obtained from the appropriate HPF model.

CHAPTER 2. LITERATURE REVIEW

2.1 Laminar Flow

The particulate heat exchanger usually has a small velocity at the inlet and plug flow in the passages. Therefore, a laminar flow with a low viscosity might be an alternative approach of modeling the moving packed bed, ignoring the particle-to-particle interaction, and treating the particulate flow as one homogenous flow by using its material bulk property.

Laminar flow can be categorized with Reynold's number. For internal laminar flow, Re < 2000. And Re can be calculated by Equation 1,

$$Re = \frac{\rho D_H U}{\mu} \tag{1}$$

where ρ is flow density, D_H is hydraulic diameter, U is mean velocity, and μ is dynamic viscosity of the fluid. For a fully-developed laminar flow, the velocity profile across the flat channel is parabolic, and the profile will not change as the flow move downstream.

The hydrodynamic entry length is the distance of a flow travels before it is fully developed. For a fully-developed laminar flow, the velocity profile is a parabola. The entry length for internal laminar flow can be calculated with Equation 2 [5],

$$L_{h,laminar} = 0.05 Re D_H \tag{2}$$

For a particulate plug flow, the velocity profile across the channel should be uniform. Therefore, a laminar flow with a very low viscosity will lead to a large Reynold's number and the resulting entry length will be large, keeping the flow from even beginning to develop into a parabola velocity profile. Such approach could be an alternative of modeling moving packed beds. This thesis shows this approach was successful.

Heat transfer of fully-developed laminar flow between parallel plates with uniform heat flux (UHF) or uniform wall temperature (UWT) has been studied practically with Nusselt Number (Nu) as well as heat transfer coefficient. Nu can be calculated by Equation 3,

$$Nu = \frac{hD_H}{k} \tag{3}$$

where h is the heat transfer coefficient and k is the thermal conductivity. Two important theoretical results are available for first testing this approach. For a fully developed flow, the theoretical Nusselt number for laminar flow in flat channel with UHF is 8.235 [6-8]. The theoretical Nu for laminar flow in flat channel with UWT is 7.541 [7]. These theoretical Nusselt numbers will be compared with the laminar flow simulation results later as a verification of the model's validity.

2.2 Plug Flow

A plug flow is an internal flow that has a constant velocity profile across any cross-section. The plug flow assumes there is no boundary layer at the wall, indication zero viscosity. The heat transfer in particulate heat exchanger has restricted movement through

a confined area. Therefore, the concept of plug flow has great potential to be an alternative of modeling the heat transfer in a particulate heat exchanger. The analytical Nusselt number for plug flow in flat channel with UHF is 12 [9], and the hydraulic diameter is calculated as twice of the spacing between parallel plates. This theoretical result was the basic for a further test. This theoretical Nusselt number will be compared with the Euler flow simulation result later to justify the model's validity. Laminar unmixed flow in the entry length has all the important kinematic features as a plug flow of a particulate.

2.3 Euler Inviscid Flow

A rigorous inviscid flow is known as an Euler flow or Euler inviscid flow for emphasis. The N-S equations simplify to the Euler equations for zero viscosity. Assuming a near zero viscosity gives an adequate approximation to the inviscid flow if the numerical analysis allows a sufficiently low viscosity. Comparison of the results in this thesis with results from an Euler inviscid flow model would be desirable but not necessary. Unfortunately, no rigorous Euler inviscid flow model was readily available for this research, so comparison with an inviscid model is deferred for later.

2.4 Particulate Heat Exchanger Modeling

There have been many study and experiment conducted for packed beds, and particulate heat transfer coefficient has been researched. Achenbach (3) used single heated bead surrounded by particles to simulate stagnant and steaming gas flows. Molerus (4) conducted experiment that had similar geometry with PFHX and concluded the importance of near-wall thermal resistance.

However, the particulate heat exchanger has not been computationally investigated widely enough. Vargas (7) has created a discrete element model for evaluating “granular systems under static and slow flow conditions”. He determined that the heat transport process depends on shear rate with conduction dominating the lower shear rates and convection dominating the higher shear rates. More recently, Albercht and Ho [10] conducted computational simulation of particulate heat exchanger with: particulate flow and sCO2 flow.

In this thesis, one-fluid model focusing only on the heat transfer of the particulate flow will be investigated. And the results will be compared with the two-fluid model. Since for a nearly-inviscid particulate flow in heat exchanger, the particle dynamics is not the priority. Thus, the heat transfer in the fluid will be focused.

Actually only one experimental investigation in the literature is consistent with this investigation since only Nguyen [1] has tested the heat transfer in a moving packed bed with a particle having a known and measured bulk thermal conductivity.

2.5 Thermal conductivity of particulates and the measurement

The moving packed bed represented by the HPF was simulated with constant density equal to the measured bulk density of the particulate. Ultimately two particulates were studied Riyadh White Sand (RWS) and industrial silica sand representative of silica sands available in a region with good potential for CSP and ID50 an alumina based foundry product representative of alumina based particulates that might be especially suitable for CSP applications. The bulk density is measured with a scale and a graduated cylinder. The bulk thermal conductivity for both was measured directly with a commercial transient

heated probe device, which should approximate the actual conductivity of the bulk particulate. For RWS the volumetric heat capacity was measured with the KD2 Pro Thermal Properties Analyzer by Decagon Devices Inc., utilizing the TR-1 and SH-1 probes [11]. The measured volumetric heat capacity was used herein as being more consistent with a hypothetical fluid model for the moving packed bed. For ID50, the mass-based heat capacity has been measured with high accuracy differential scanning calorimeter methods [12].

CHAPTER 3. COMSOL MODELING AND SIMULATION RESULTS

The CFD modeling is trivial but interpreting the HTF results is somewhat demanding because it is necessary of the user to accurately compute the mixed fluid temperature. To verify this computation, some simple cases were run and compared with analytical results.

3.1 Preliminary Model: Air Flow between Parallel Plates

Flow of air and other similar fluids with constant properties has been thoroughly studied between parallel plates. Hence, air is used first to first test the validity of modeling heat transfer flows between parallel plates. In addition, with both laminar flow and Approximate Euler flow simulation, the results of air flow simulations, in particular the Nusselt number, will be used to compare with the analytical result to prove the validity of the model.

In the following modeling and simulation, air with constant properties flow through a flat channel with uniform heat flux at the wall.

3.1.1 Model Settings and Geometry

Air with constant property enters in the flat channel with a velocity of 0.01 m/s and room temperature from the top of the geometry, as shown in Figure 1. A uniform heat flux of 100 W/m^2 is applied at both walls. The spacing between the parallel plates is 0.04 m and the channel length is 0.114 m. The Re calculated by Equation 1 was 52.97, confirming that

the flow is laminar. Air enters in the parallel heat exchanger from the top and exits at the bottom. The mesh independence is verified for the following results.

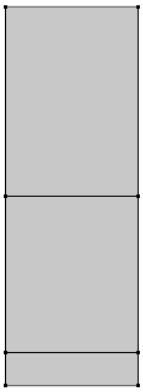

Figure 1 – Model geometry of laminar air between parallel plates (0.114 m by 0.04 m).

Note, the lines across the middle and near exit are used to generate velocity profiles and heat transfer coefficients across the midstream and downstream, and they do not interfere the fluid dynamics and/or fluid heat transfer.

3.1.2 Simulation Results with Laminar Flow Module

Firstly, the Reynold's number calculated with Equation 1 is 53.26, and entry length calculated with Equation 2 is 0.213 m. This means the flow is obviously laminar, but it might still not have become fully developed. To illustrate this, the simulated velocity profiles across midstream and downstream are shown in Figure 2. Since the entry length is the same order of magnitude as the passage length, the flow is expected to be nearly fully

developed across the midstream. A passage much longer than the entry length was also tested to confirm these results. Therefore, as expected, the velocity profiles are parabola, and the midstream velocity is almost the same as that of the downstream, as the model has a uniform velocity at the input and a short entry length

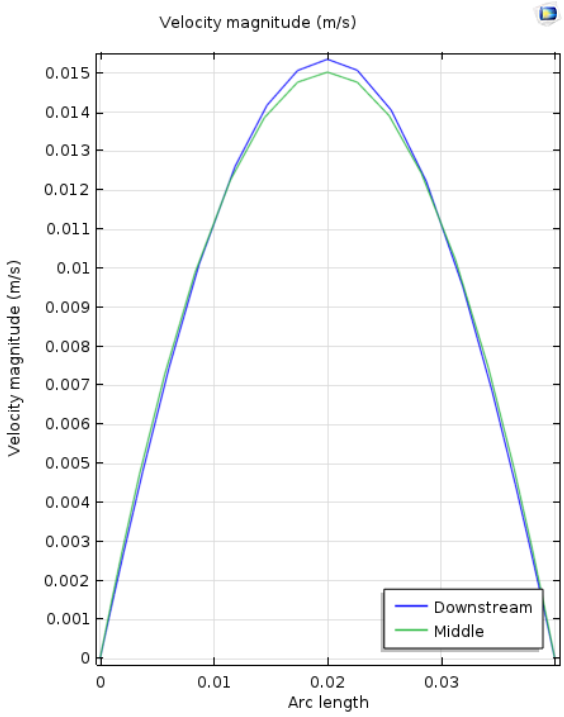

Figure 2 – Velocity profile of laminar air flow in UHF flat channel

Viscosity = 1.81×10^{-5} Pa-s

To verify the heat transfer results of the model, the heat transfer coefficient using Equation 4-5, and corresponding Nusselt numbers are calculated with Equation 3.

$$h = \frac{\dot{q}}{T_{wall} - T_m} \tag{4}$$

$$\dot{m} \cdot Cp \cdot T_m = \int U \cdot Cp \cdot \rho \cdot T \cdot dA \tag{5}$$

where h is heat transfer coefficient, $\dot{q}$ is inward heat flux, T_{wall} is the wall temperature at where the heat transfer coefficient is desired (in this case, wall temperature at middle and downstream in Figure 1) , T_m is the mixed temperature, $\dot{m}$ is mass flow rate, Cp is heat capacity, U is flow velocity and ρ is density. Equations 5 is important as it computes the very important mixed fluid temperature needed in heat transfer analysis.

Table 1 presents both the simulated results and the theoretical results. The simulated results agree with the theory very well, indicating the model is relatively accurate and is ready for plug flow simulation. Table 1 confirms that accurate heat transfer results are returned by this model, the expected result.

Table 1 – Nu and heat transfer coefficient of laminar air flow in UHF flat channel

	h [W/K-m^2]	Nu
Middle	2.660	8.279
Downstream	2.663	8.289
Theory	2.645	8.235

3.1.3 Simulation Results with Euler-Euler Flow Module

The model is then tested for plug flow with very low viscosity air flow in UHF parallel wall channel. In laminar module, the smallest viscosity allowed for air with constant property is at the order of 10^{-6}. For lower viscosity, the laminar model would not converge. Therefore, instead of laminar flow, Euler-Euler flow with continuous phase only was applied to model inviscid flow because it was found that only the approximate inviscid Euler flow model successfully modeled a plug flow. The same

geometry is the same as Figure 1, and the viscosity is set to be vanishingly small (*i.e.* order of 10^{-10}). Figure 3 plots the velocity profile for both midstream and downstream. As shown in the figure, the velocity boundary layer is negligible, a nearly-inviscid flow property. The midstream velocity profile is exactly the same as that of the downstream. Figure 3 shows that the kinematics of a plug flow is captured with this model.

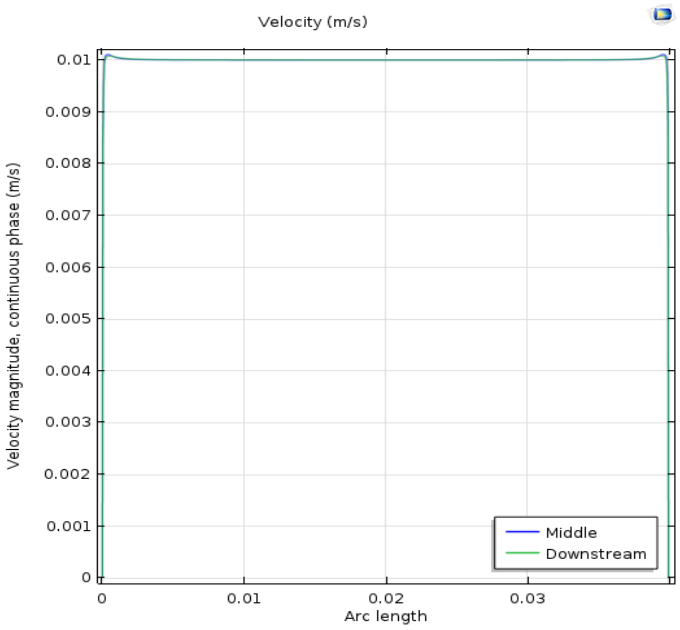

Figure 3 – Velocity profile of plug air flow in UHF flat channel Euler Model Viscosity = 1.81×10^{-10} Pa-s

To test the heat transfer coefficient of model, the heat transfer coefficient calculated with Equation 4-5 and corresponding Nu calculated with Equation 3 are compared with analytical results shown in Table 2. The simulated results show almost prefect agreement

with the analytical plug flow result, indicating the model is accurate and is ready for particulate moving bed simulation.

Table 2 – Nu and heat transfer coefficient of plug air in UHF flat channel

	h [W/K-m^2]	Nu
Middle	3.853	11.993
Downstream	3.852	11.991
Theory	3.855	12.000

3.2 Hypothetical Particulate Flow (HPF) between Parallel Plates

The property of ID50 is used as a potential particulate for heat exchanger because its thermal properties has been verified with previous experiment [1]; in addition, ID50 will used in the proposed design of particulate heat exchanger in the later chapter. The model geometry is the same as in Figure 1. Sand enters in the parallel heat exchanger from the top and exits at the bottom. The material viscosity is set to be nearly zero to model the constant velocity profile across any cross-section. The mesh independence is verified for the following results.

3.2.1 Simulation Results with Euler-Euler Flow Module

The parallel plate geometry was then further modified so as the hydraulic diameter is the same as that of the particulates moving bed experiment. The velocity profile was first examined, as shown in Figure 4.

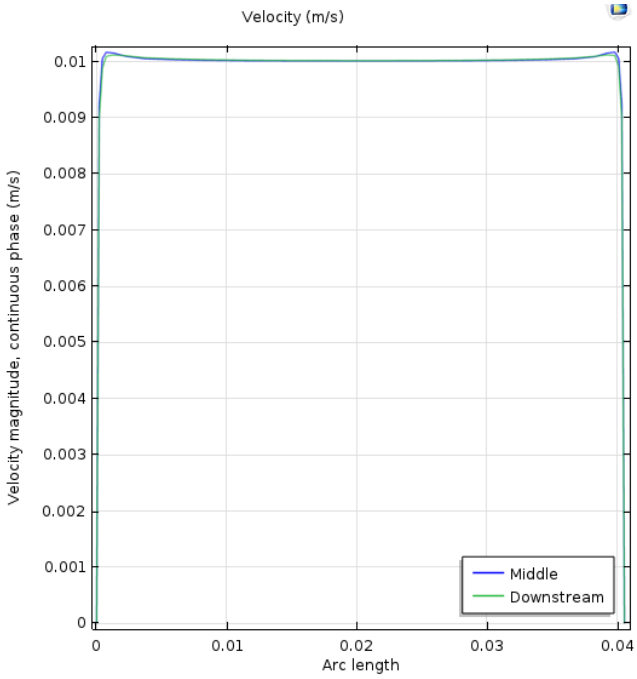

Figure 4 – Velocity profile of HPF particulates flow in UHF flat channel

Euler Model Viscosity = 1.81×10^{-10} Pa-s

Again, the heat transfer coefficient and corresponding Nu are calculated for this model. The theoretical Nu is 12 for fully developed flow thermally, and the hydraulic diameter is calculated as twice of the spacing between parallel plates. Table 3 presents both the simulated results and the theoretical results. The simulated results agrees with the theory very well, indicating the model is accurate and is ready for particulates moving bed simulation with more accurate geometry.

Table 3 – Nu and heat transfer coefficient of particulate flow in UHF flat channel

	h [W/K-m^2]	Nu
Middle	32.268	11.841
Downstream	32.251	11.835
Theory	32.700	12.000

3.3 Verifying the Bulk Thermal Conductivity of Particulate

For the previous sections, Riyadh White Sand bulk property is used for the HPF. When the sand is behaved as a bulk fluid, the bulk property differs from the individual particulate property. Thus, to further test the HPF material modeling results, a model is designed to duplicate experimental results [1]. In the experiment, sand flows into a heat exchanger box has inner dimensions of 0.114 m by 0.114 m by 0.114 m. eight cartridge heaters with 15.875 mm in diameter, 101.6 mm in length, providing 200 Watts at 120 VAC are inserted in the box as shown in Figure 5. The measured heat transfer coefficient is 100 $W/(m^2K)$ with thermal conductivity of 0.290 W/(mK). The mesh independence is verified for the following results.

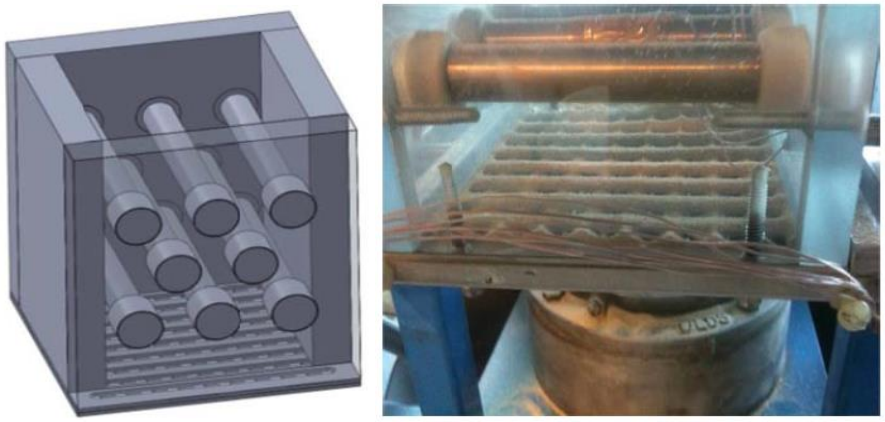

Figure 5 – Heat exchanger component (left) Heat exchanger side view (right)

3.3.1 Model settings and Geometry

The middle section of the heat exchanger is modelled to verify the heat transfer coefficient with the experimental results. To save computational cost, the model is only constructed in half with symmetric condition along the right side of the geometry, shown in Figure 6. The length of this segment is 0.114 m, the width is 0.019 m, with a heat flux of 39,490 W/m^2 at curved surfaces. The inlet velocity of the sand is 0.01 m/s and the sand enters with a temperature of 313.15 K from the top and exits at the bottom.

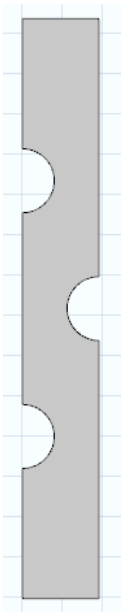

Figure 6 – Heat exchanger geometry

3.3.2 Simulation Results with Laminar Flow Module

The model is first simulated with laminar flow module. Although the temperature surface, shown in Figure 7, suggest a reasonable result, the velocity profile, shown in Figure 8, indicates laminar module is not suitable for plug flow, as the flow does not maintain a constant velocity profile across the cross-section. In addition, the calculated heat transfer coefficient does not agree with the experimental measured result. Thus, laminar flow module is not suitable for modeling plug flow with more complexed geometry.

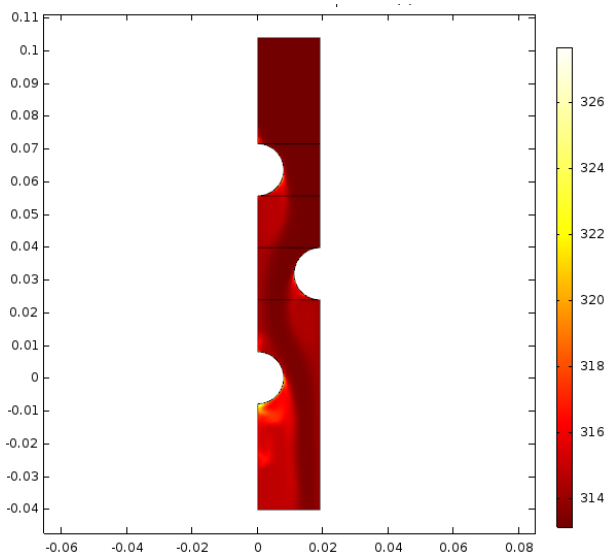

Figure 7 – Laminar flow temperature surface of the heat exchanger

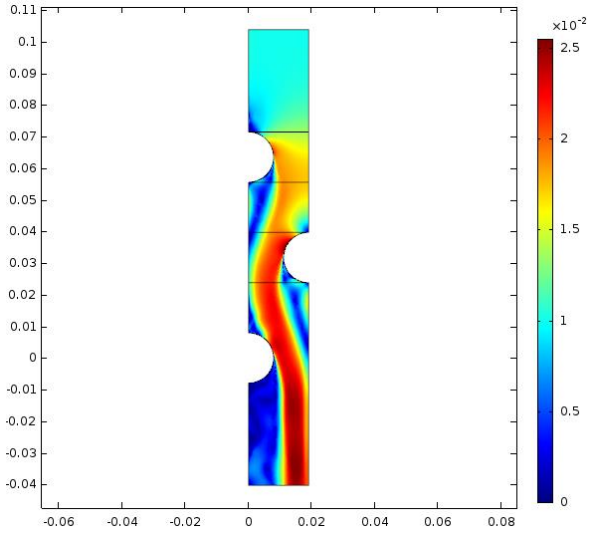

Figure 8 – Laminar flow velocity surface of the heat exchanger

3.3.3 Simulation Results with Euler-Euler Flow Module

The same geometry is then simulated with Euler-Euler laminar flow module with active continuous phase only. The temperature surface is plotted in Figure 9, and the

velocity surface is plotted in Figure 10. Comparing to the velocity surface of the laminar approach, the plug flow characteristics are much preserved in this approximate Euler flow approach. In addition, the flow pattern is just as observed in the experiment, with the particulate velocity being slower at the top and bottom of the heaters, and slightly faster at the side of the heaters.

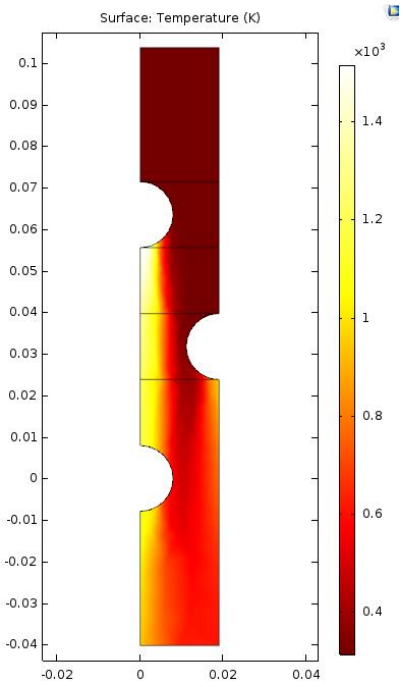

Figure 9 – Euler-Euler laminar flow temperature surface of heat exchanger

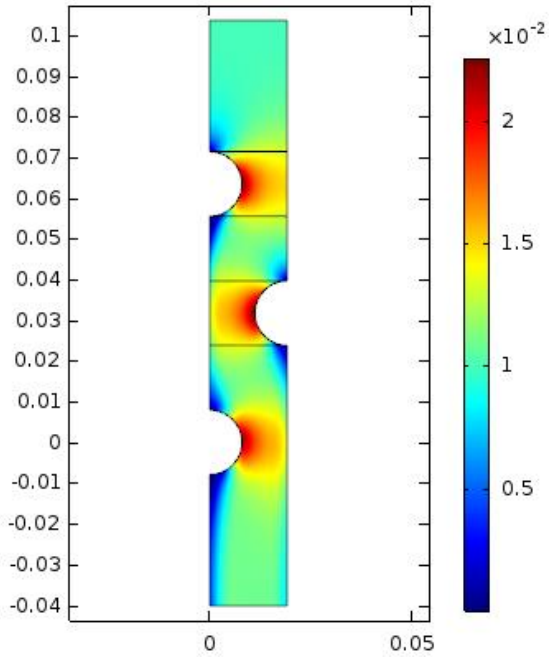

Figure 10 – Euler-Euler laminar flow velocity surface of heat exchanger

The heat transfer coefficient is calculated from the simulation using the following Equation 6-9,

$$h = \frac{\dot{q}}{T_{heater} - T_m} \tag{6}$$

$$\dot{m} \cdot Cp \cdot T_1 = \int U \cdot Cp \cdot \rho \cdot T \cdot dA \quad \text{(at location 1)} \tag{7}$$

$$\dot{m} \cdot Cp \cdot T_2 = \int U \cdot Cp \cdot \rho \cdot T \cdot dA \quad \text{(at location 2)} \tag{8}$$

$$T_m = 0.5 \cdot (T_1 + T_2) \tag{9}$$

where T_{heater} is the average temperature at the curved surface representing cartridge heaters, Location 1 is the horizontal cross section at the top of the first curved surface and location 2 is the horizontal cross section where the first curved surface ends. The heat

transfer is calculated to be 127.95 W/(m^{2}K), yielding a 7.64% of difference of the experimental measured result.

Furthermore, the mass and energy balances are verified for this model using Equation 10 – 13, where $\dot{H}$ is the enthalpy flow. Since the elevation is small, the potential energy is neglected. And the kinetic energy should be the same at the inlet and exit, due to plug flow characteristics, and the inlet and exit have the same cross-sectional area, the dominating energy in this model is in the form of heat. Therefore, the energy balance is checked in the form of enthalpy balance.

$$\dot{m}_{in} = \dot{m}_{out} \tag{10}$$

$$\dot{m} = \int \rho U \, dA \tag{11}$$

$$\dot{H}_{in} + \dot{Q}_{heater} = \dot{H}_{out} \tag{12}$$

$$\dot{H} = \int \rho U C p T \, dA \tag{13}$$

The mass flow rates are summarized in Table 4, where the mass flow difference, Δ, calculated by the mass flow rate at the exit minus that of the inlet, is only 0.00099 kg/s, which is only 0.003% comparing to the magnitude of the mass flow rate. Therefore, it can be conclude that the mass is balanced in model.

Table 4 – Mass balance check

$\dot{m}_{in}$ [kg/s]	$\dot{m}_{out}$ [kg/s]	Δ [kg/s]	Δ%
0.29737	0.29836	0.00099	0.00333

Similarly, the enthalpy flow rates and heat flow rate are summarized in Table 5. The ϵ is the error in the energy balance, which is calculated by $\dot{H}_{in} + \dot{Q}_{heater} - \dot{H}_{out}$. Although the value error may seem to be significant, comparing to the magnitude of enthalpy flow rate, it is only -0.003%. Therefore, it can be conclude that the energy is balanced in model.

Table 5 – Energy balance check

$\dot{H}_{in}$ [W]	$\dot{H}_{out}$ [W]	$\dot{Q}_{heater}$ [W]	ϵ [W]	ϵ%
78688	81943	3019.6	-235.4	-0.00299

3.3.4 Simulation Results with Other HPF

Other particulate flows besides RWS have also been tested in the above box heat exchanger [1]. With the same modelling geometry, ID50, Atlanta Industrial Sand (ATL), CarboHSP, and Arizona Fracking Sand (AFS) are simulated with an inlet velocity of 10 mm/s. Table 6 summarizes the material thermal properties used for each HPF in the simulation, as well as the comparison between the measured heat transfer coefficient and the simulated results. Only CarboHSP has a big difference in the heat transfer coefficient, which could due to systematic errors or human errors in the experiment. However, overall, the model accurately represents the heat transfer process for most of the HPFs, and the simulated heat transfer coefficients are within 10% of difference of the measured values in the experiments. Thus, it is reasonable to conclude that this model is capable of represent the heat transfer of the HPF equivalently.

Table 6 – HPF experimental results compared with simulation

	RWS	ID50	ATL	CarboHSP	AFS
$k_{measured}$ [W/m-K]	0.290	0.220	0.226	0.263	0.250
Cp [kJ/kg-K]	0.846	0.885	0.824	0.855	0.779
ρ [kg/m^3]	1561	1823	1364	2152	1581
Volumetric Cp [MJ/m^3-K]	1.320	1.613	1.124	1.839	1.232
$h_{measured}$ [W/K-m^2]	118.87	114.17	107.28	105.09	110.20
$h_{simulated}$ [W/K-m^2]	127.95	123.8	113.8	133.46	121.03
Δh %	7.64	8.43	6.08	27.00	9.83

3.4 Conclusion

Comparing the laminar module and Euler-Euler laminar module, the Euler-Euler laminar module is more suitable to model a plug flow because it converges to a solution at a sufficiently low viscosity to preserve the constant velocity profile. Moreover, the Euler-Euler laminar module enables a two-phase flow with continuous phase and dispersed phase, which conceivably could be helpful in modelling particulate flowing with a free surface as in the zig-zag flow exchanger described later. Therefore, for the following particulate heat transfer modelling, the very low viscosity Euler-Euler laminar module will be used.

In addition, the box heat exchanger model agrees with the experimental results, indicating that in moving packed beds the measured bulk thermal conductivity does apply.

CHAPTER 4. COMSOL MODELING OF PARTICULATE HEAT TRANSFER

4.1 Preliminary Model: Straight

4.1.1 Model Settings and Geometry

The preliminary approach is to model the heat exchanger as 2-D hypothetical fluid flow between 4 sets of parallel plates in series, as shown in Figure 11. The walls are set to be at constant temperatures, where the temperatures are the average temperature of the CO_2 corresponding to each bank in the SunLamp report [3], summarized in Table 7. The hypothetical fluid is set to be a plug, nearly inviscid flow by using the continuous phase in Euler-Euler flow module. The thermal conductivity of the hypothetical fluid is set to be constant (0.220 W/m/K). Sand (ID50) enters in the parallel heat exchanger from the top and exits at the bottom. The mesh independence is verified for the following results.

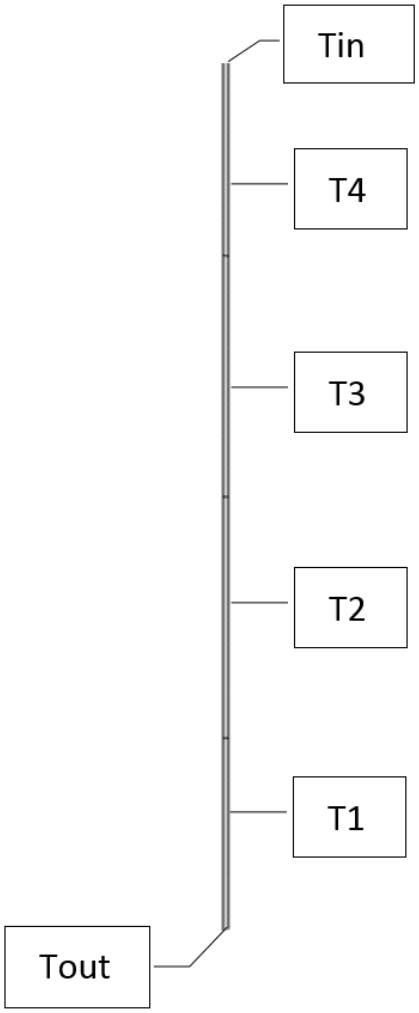

Figure 11 – Model geometry of straight channel heat exchanger

4 banks; each bank has 0.254 m in length and 0.00635 m in width

Table 7 – Temperature inputs of straight channel heat exchanger

Tin (K)	T1(K)	T2(K)	T3(K)	T4(K)
1048.20	831.45	853.40	889.70	945.90

4.1.2 Simulation Results

The simulation results are in consistent with those of the SunLamp report [3]. The temperature and velocity surfaces are shown in Figure 12. The hypothetical fluid exiting temperature is simulated to be 841.15 K. The comparison between the simulation and data provided by SunLamp is summarized in Table 8.

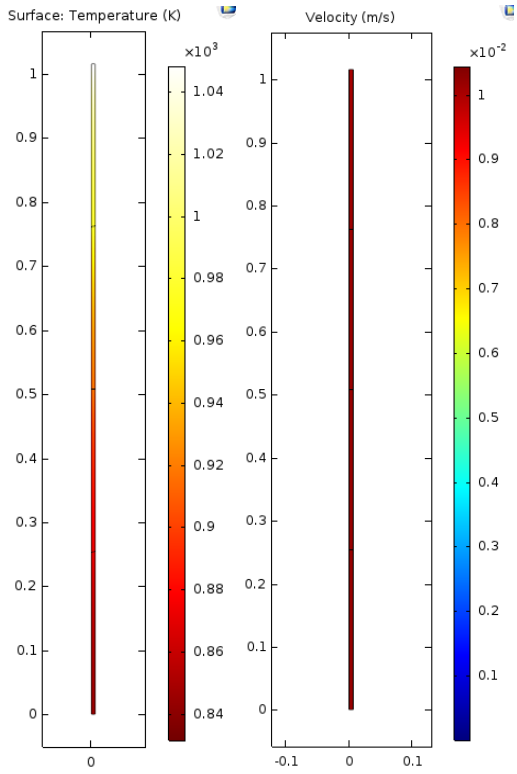

Figure 12 – Preliminary simulation results: Temperature Surface (Left) and Velocity Surface (Right)

Table 8 – Results comparison between preliminary model and SunLamp report

	Tin [K]	Tout [K]	dT [K]		
Simulation	1048.2	841.15	207.05		
SuNLaMP-0000000-1507	1048.2	832.65	215.55		
				Difference %	-3.94

4.2 Offset Model

In the SunLamp design, there is an offset between banks, which enhances thermal entry and causes the spikes in the temperature between banks, as shown in Figure 13 and Figure 14. The mesh independence is verified for the following results.

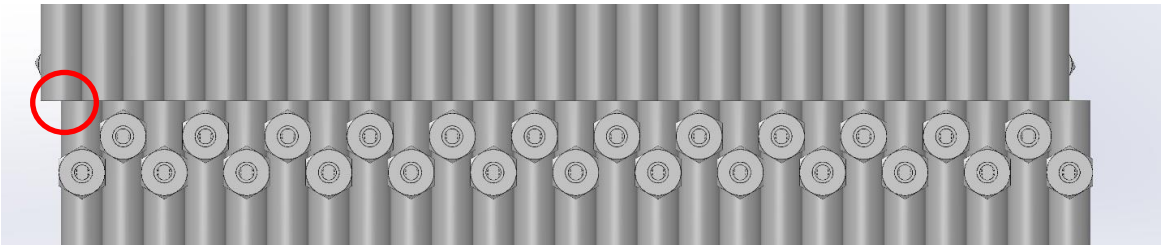

Figure 13 – Offset between Banks[3]

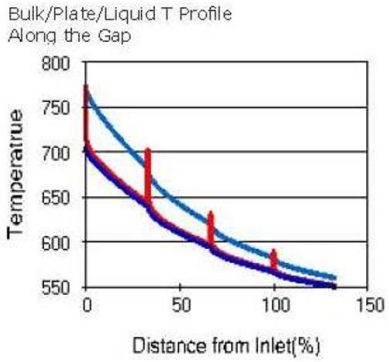

Figure 14 – Temperature profile along the banks[3]

4.2.1 Model Settings and Geometry

To further improve the model, geometry is modified first to make the model more realistic. Figure 15 presents the modified geometry with a close up at the bank transition.

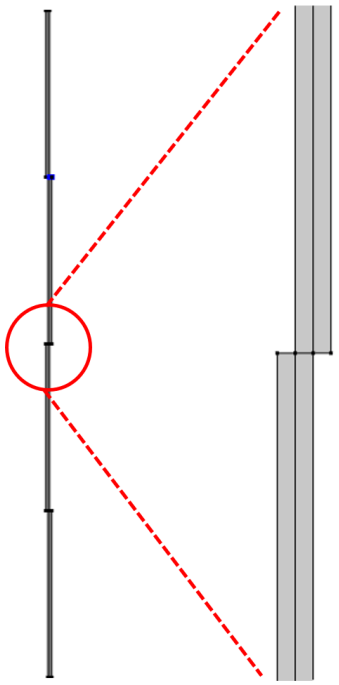

Figure 15 – Offset model geometry and close-up (Right)

Note, the lines across each bank are used to set the boundary similarity, and they do not interfere the fluid dynamics and/or fluid heat transfer.

To model the offset, a boundary similarity condition is imposed at the bank transitions. In general, the right side of the second bank is receiving fluid from the left side of the first bank that is next to the modeled plate. Since the plates are parallel with the same boundary condition, the profile of the left side of the first bank that is next to the modeled plate should be the same as the left side of the first bank. Therefore, the entrance of the right side of the second bank (show in pink in Figure 16) would use the temperature and velocity profile of the exit of the left side of the first bank (show in orange in Figure 16). Such boundary condition is applied between all bank transitions.

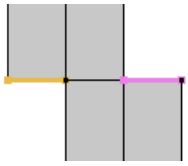

Figure 16 – Offset Model Boundary Similarity

4.2.2 Simulation Results

To test validity of the boundary similarity condition, the velocity and temperature profile are plotted at both the orange and pink segments, shown in Figure 17 and Figure 18 correspondingly. The following figures state that the velocity profiles at the modified segments are exactly overlapping, and the temperature profiles are almost overlapping. Therefore, this boundary condition is valid for solving the offset problem.

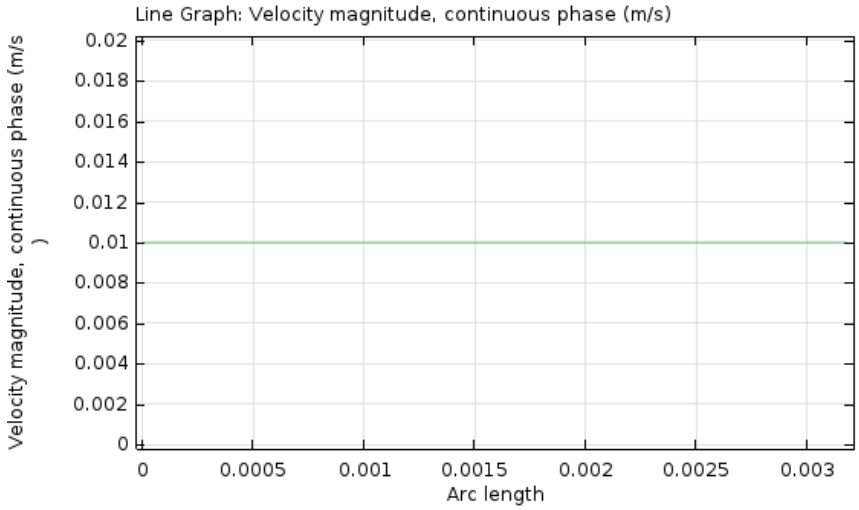

Figure 17 – Offset model velocity profile at boundary similarity segments

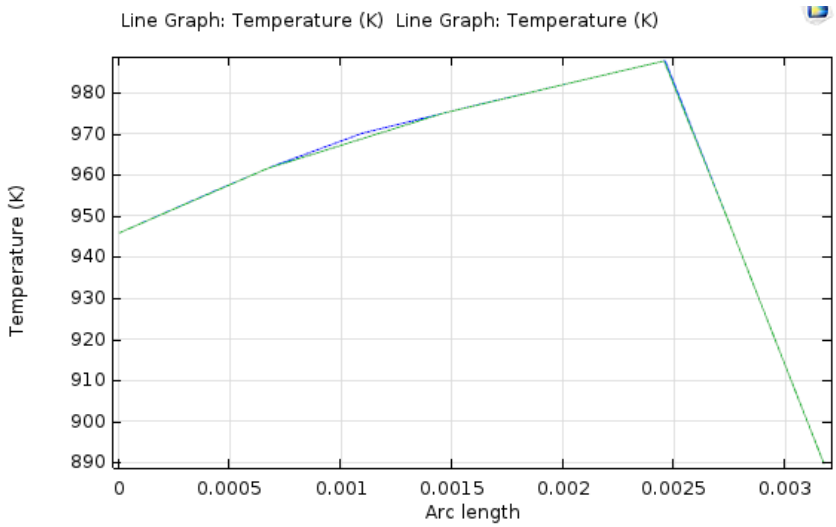

Figure 18 – Offset model temperature profile at boundary similarity segments

To further investigate the offset influence on the temperature profile, the temperature profile across middle of the first bank is plotted in Figure 19. As expected, the wall cools down the HPF and thus the temperature profile is a parabola.

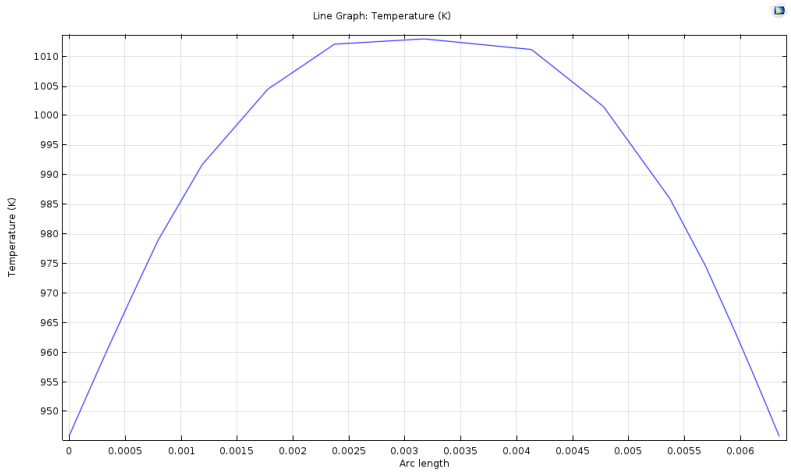

Figure 19 – Temperature profile across the middle of the first bank (Offset model)

The temperature profile is also plotted right below the entry of the second bank, as shown in Figure 20, to check the offset effect. The temperature at the walls is still cooling the HPF, yet there is a small pit in the center of the temperature profile. This is because the temperature at the center near entry still preserve the profile shape (parabola) from previous banks; with the offset, they create a pit in the center, as Figure 21 illustrates.

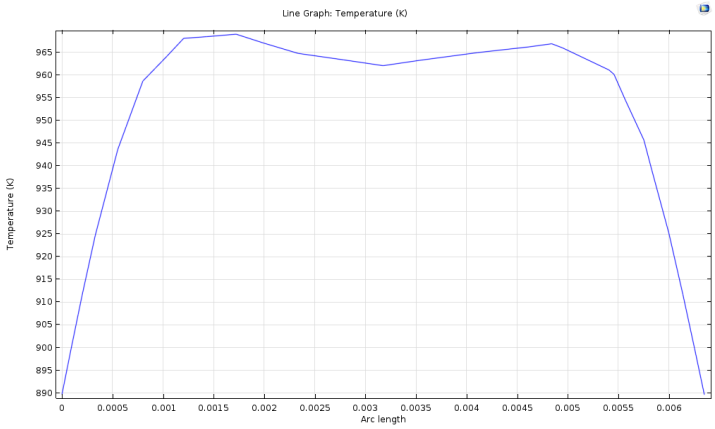

Figure 20 – Temperature profile across the entry of second bank (Offset model)

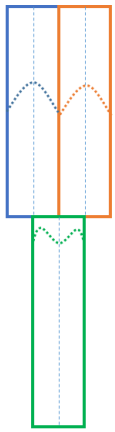

Figure 21 – Illustration of temperature profile changes from first bank to second bank (Offset model)

Again, the simulation results are in consistent with those of the SunLamp report [3]. The temperature and velocity surfaces are shown in Figure 22. The hypothetical fluid exiting temperature is simulated to be 840.1 K. The comparison between this simulation and data provided by SunLamp is summarized in Table 9.

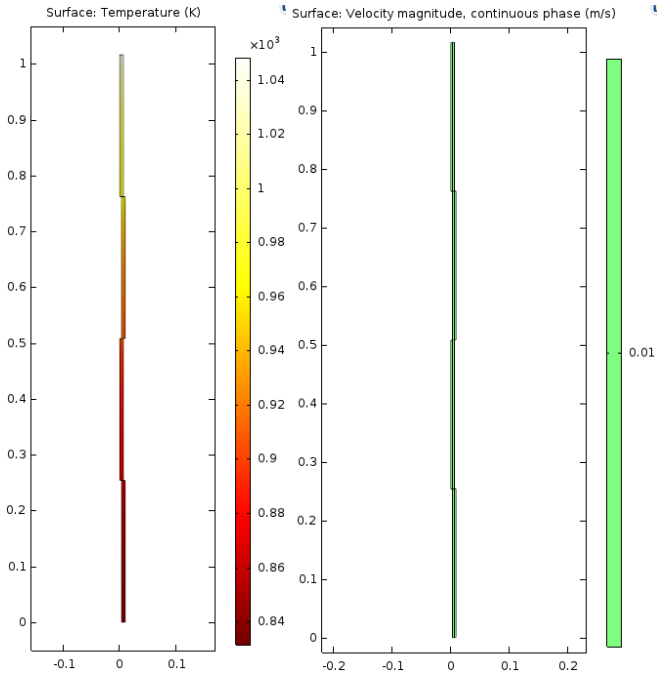

Figure 22 – Offset model temperature surface (Left) and velocity surface (Right)

Table 9 - Results comparison between offset model and SunPos report

	Tin [K]	Tout [K]	dT [K]		
Offset Model	1048.2	840.1	208.1		
SuNLaMP-0000000-1507	1048.2	832.65	215.55		
				Difference %	-3.46

Figure 23 presents the temperature profiles plotted across all 4 banks, from inlet to exit, for the offset model and Figure 24 presents the temperature profiles plotted across the centerline of preliminary straight model. Figure 25 illustrates the cutline in red where the temperature profile in Figure 23 is plotted. The cutline is located at the middle of the right half of the first bank from the inlet, and enters the second bank at the middle of its left half due to geometry offset; then it is located at the middle of the right half of the 3 bank and again at the middle of the left half of the fourth bank. By comparsion, the offset modified model has more spikes at the bank transitions and is more similar to that of the SunLamp results shown in Figure 14.

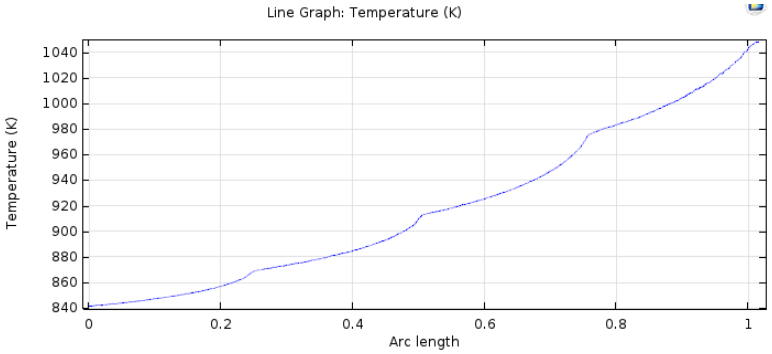

Figure 23 – Offset model temperature profile along the bank

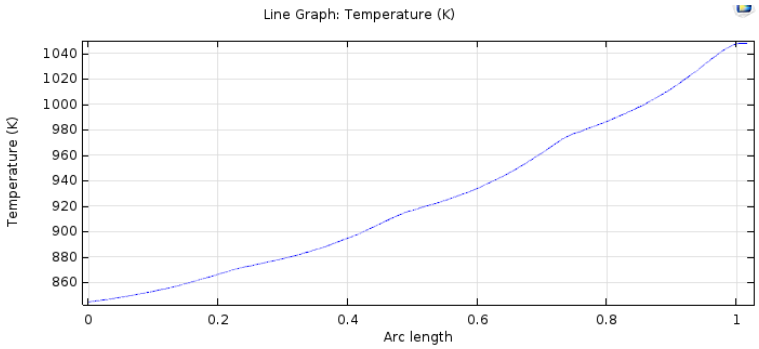

Figure 24 – Perliminary model temperature profile along the bank

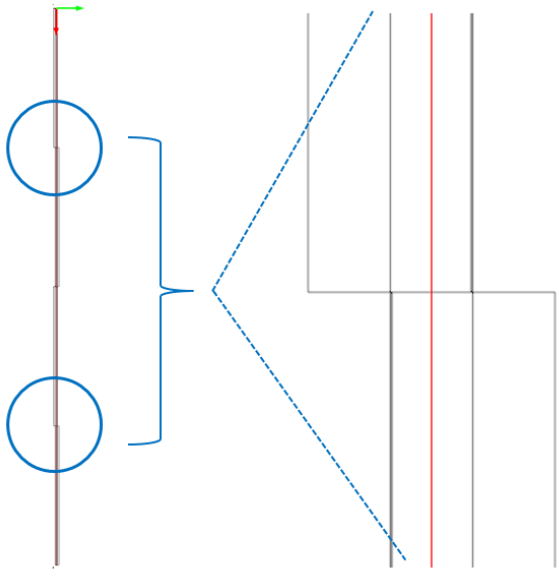

Figure 25 – Cutline (in red) for Temperature Profile across the banks

4.3 Near-Wall Resistance

Comparing to the moving packed-bed, heat transfer is reduced at between the particles and the walls of particulate flow because the particle near the wall is surrounded by less particles than those in the middle of the moving paced-bed. Assuming perfectly spherical particles, a single particle can be close-packed by 12 other particles for a dense packing without overlapping, shown in Figure 26. Therefore, with one side “blocked” by the wall, the particle will lose at least 2 particles in contact for heat transfer.

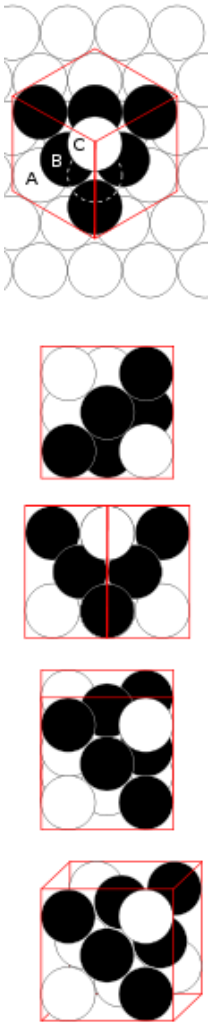

Figure 26 – Face centered cubic (FCC) lattice packing [13]

To accommodate this particulate flow behavior, the thermal conductivity at the wall is suggested to be adjusted [10, 14]. Patil et al. [15] suggested the near-wall void fraction modification in thermal conductivity for both solid and fluid of particulate flow in Equations 14 to 19

$$k_{f,eff} = \left(\frac{1-\sqrt{\alpha_s}}{\alpha_f}\right) k_f \tag{14}$$

$$k_{s,eff} = \frac{k_f}{\sqrt{\alpha_s}}[0.00726A + 0.99274\Gamma] \tag{15}$$

$$\Gamma = \frac{2}{1-\frac{B}{A}}\left(\frac{A-1}{\left(1-\frac{B}{A}\right)^2}\frac{B}{A}\ln\left(\frac{A}{B}\right) - \frac{B-1}{1-\frac{B}{A}} - \frac{B+1}{2}\right) \tag{16}$$

$$A = \frac{k_s}{k_f} \tag{17}$$

$$B = 1.25\left(\frac{\alpha_s}{\alpha_f}\right)^{\frac{10}{9}} \tag{18}$$

$$\alpha_{f,wall} = \begin{cases} 1.26\alpha_f - 0.26 + 1.26(1-\alpha_f)\left(\frac{2x}{d_s} - 1\right), & \left(0 \le \frac{x}{d_s} \le \frac{1}{2}\right) \\ \alpha_f + 0.26(\alpha_f - 1)\exp\left(\frac{1}{4} - \frac{x}{2d_s}\right)\cos\left(\frac{\pi}{0.816}\left(\frac{2x}{d_s} - 1\right)\right), & \left(\frac{x}{d_s} \ge \frac{1}{2}\right) \end{cases} \tag{19}$$

where k is thermal conductivity, α is volume fraction, d_s is particle diameter, and x is distance to wall.

Such a complicated model may be used and found useful in the future, but for now to simplify the approach, a reasonable enhanced near-wall resistance is added to the model. A lower thermal conductivity is set near the wall. Note that a careful study of the mesh independence has been made and is verified for the following results.

4.3.1 Model Settings and Geometry

The model is updated to include weaker thermal conductivity at the near wall region. A thin layer of HPF with lower conductivity is added close to one side of the wall,

with the thickness of a hundredth of the bank thickness. As illustrated in Figure 27, the thickness of the low thermal conductivity thin layer is about 60 μm, smaller than that of the common particulate size (around 300 μm [1]); thus the thickness of the thin layer is reasonable.

The thermal conductivity at the thin layer (0.110 W/mK) is set to be half of the bulk thermal conductivity (0.220 W/mK).

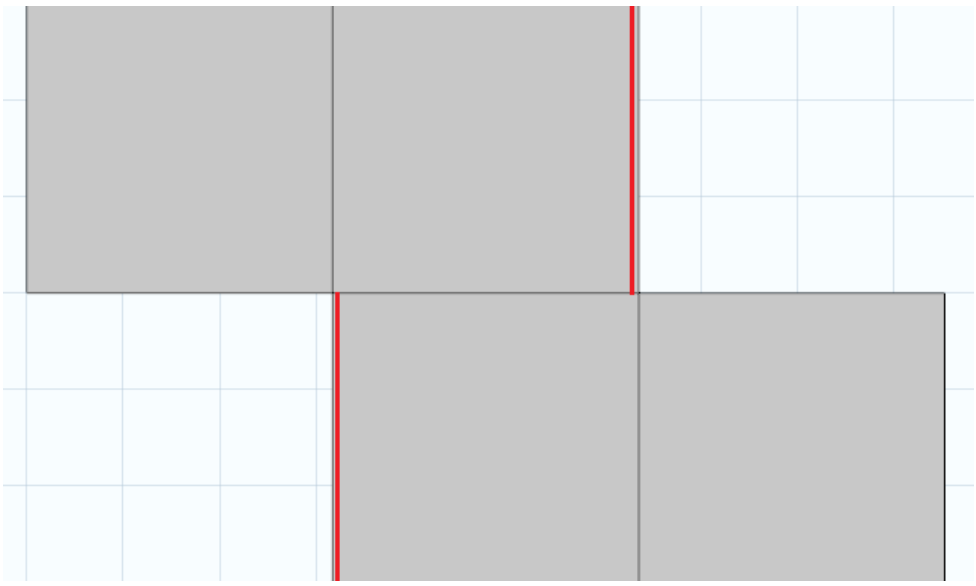

Figure 27 - Particulate heat exchanger with near-wall thermal resistance

4.3.2 Simulation Results

As the velocity is still uniform across the surface, only temperature profile is plotted as shown in Figure 28.

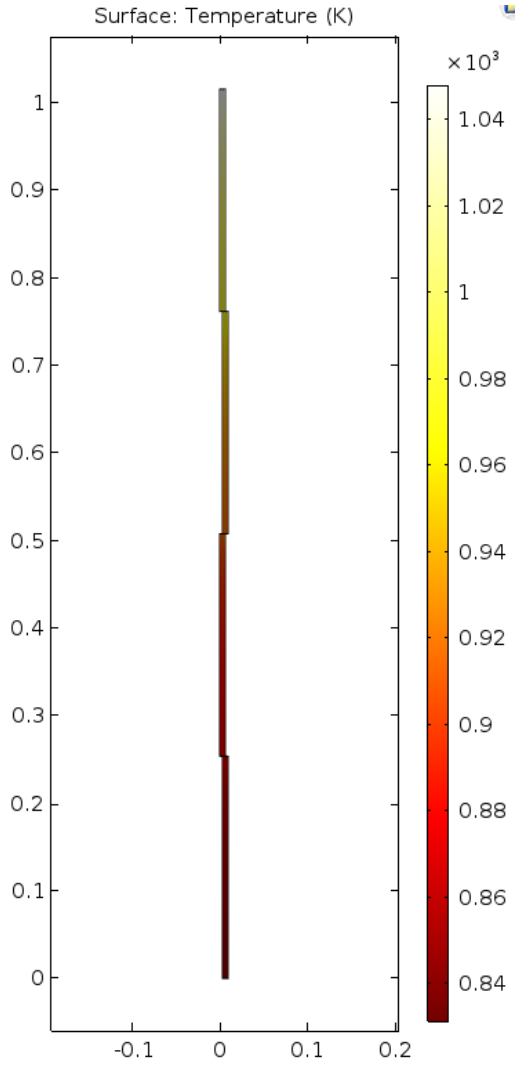

Figure 28 – Temperature surface with near-wall resistance

Comparting to previous models, the simulation results have little variation. Table 10 summarizes the average exiting temperature of the particulates of all the models.

Table 10 – Exiting Temperature Comparison of Models

	Tin [K]	Tout [K]	ΔT [K]	% Diff in ΔT
SuNLaMP-0000000-1507	1048.2	832.7	215.6	0
Preliminary Straight Model	1048.2	841.2	207.1	-3.94
Offset Model	1048.2	840.1	208.1	-3.46
Near-Wall Resistant Model	1048.2	840.9	207.3	-3.81

Figure 29 plots the temperature across the 4 banks. Comparing to the previous offset model (Figure 23), the temperature pofile does not have obvious changes, indicating the near-wall resistant has a minimal influnence in this simulation.

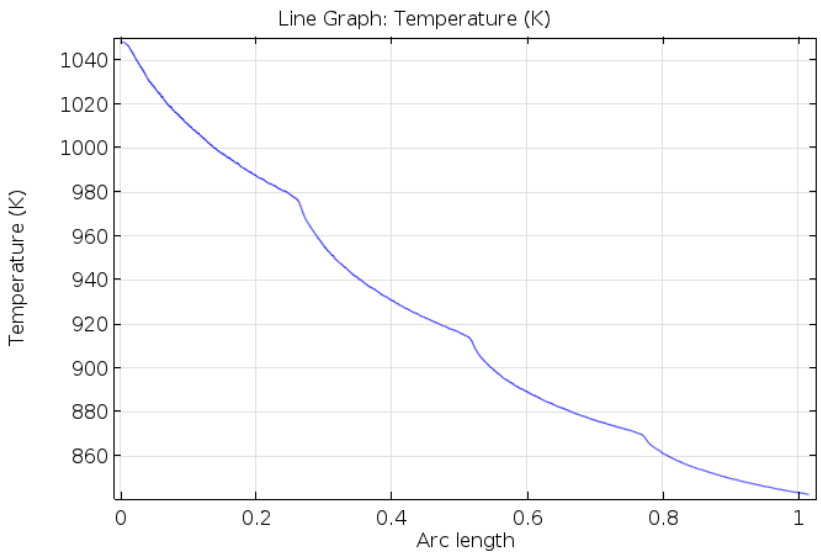

Figure 29 – Temperature profile along the bank with near-wall resistance

Figure 30 compares the temperature profiles of the second bank entry and the mid-way of the second bank. As expected, the results have no big difference than thoes of the offset model without a near wall resuistance.

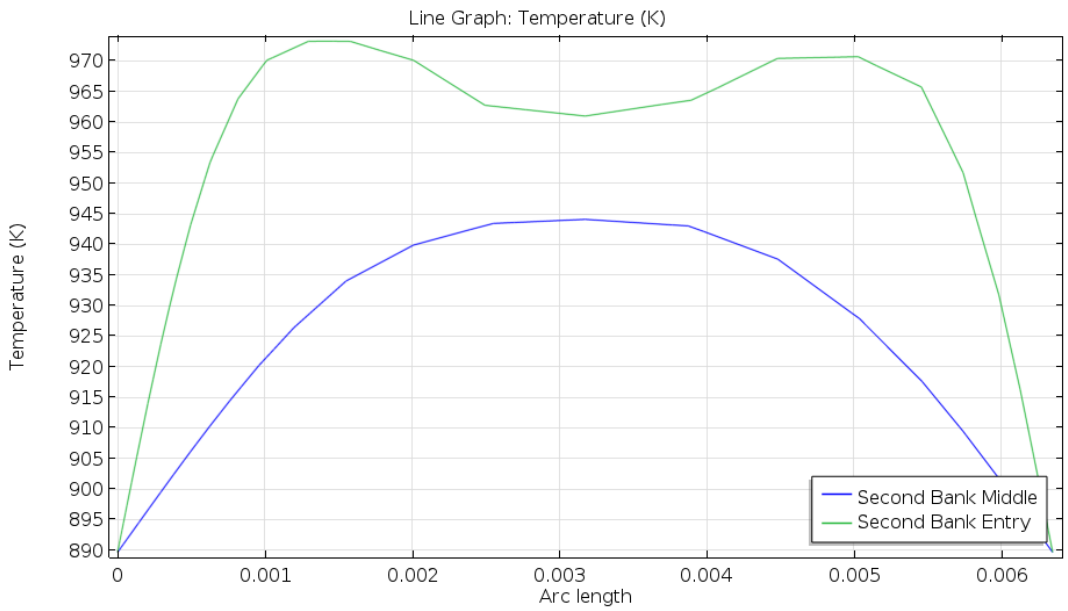

Figure 30 – Temperature profiles at the second bank

4.4 More on Heat Transfer Coefficient

The heat transfer coefficient is calculated at the middle of the first bank, using Equations similar to Equation 4-5. The resulting heat transfer coefficient is 216.44 W/m^2K, yielding a -3.38% difference with Solex's two-fluid model result [16]. Thus, the heat transfer coefficient is proven to be valid and can be used in the MATLAB network model introduced in the final chapter.

Moreover, a parametric study is conducted on the heat transfer coefficient by varying the particulate inlet velocity from 10 mm/s to 50 mm/s in step of 2 mm/s. The results are summarized in Figure 31. The heat transfer coefficient increases as the inlet particle velocity increases as expected [17].

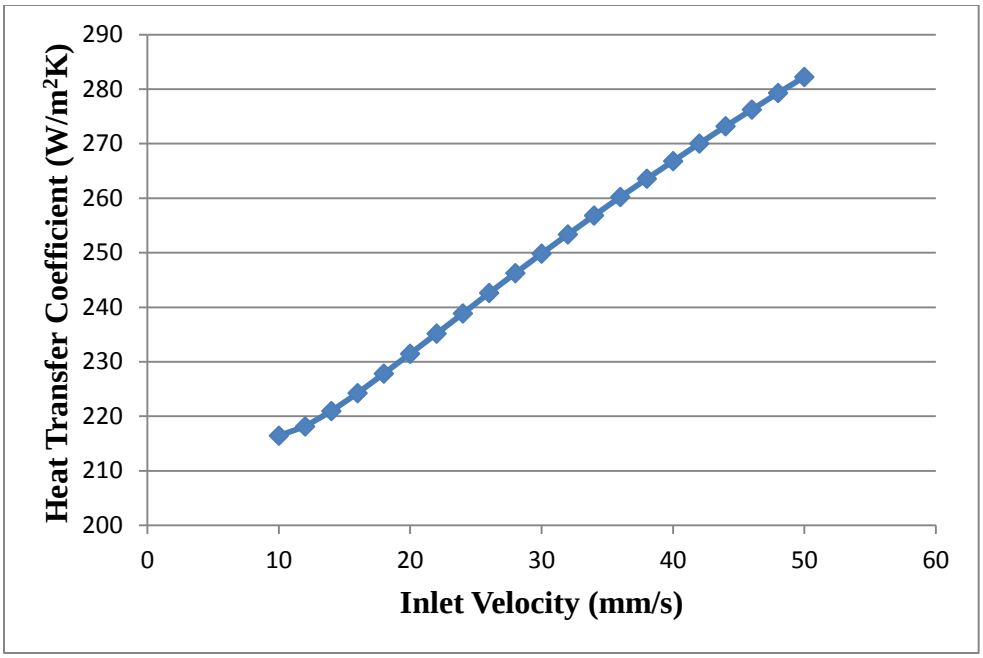

Figure 31 – Particle inlet velocity vs. Heat transfer coefficient

4.5 Thermal Conductivity varied with Temperature

The thermal conductivity of the HPF is expected to increase at higher temperature due to the conductivity of air in the HPF mixture increases strongly with temperature; in addition, the radiation of air also increases strongly with the temperature, and tends to enhance the contribution to the thermal conductivity of the bulk particulate. Although the conductivity of the solid particle may decrease with temperature, both the conductivity increase in air and radiation effect dominates, causing a general increase in bulk conductivity of HPF. Figure 32 illustrates the effect described above.

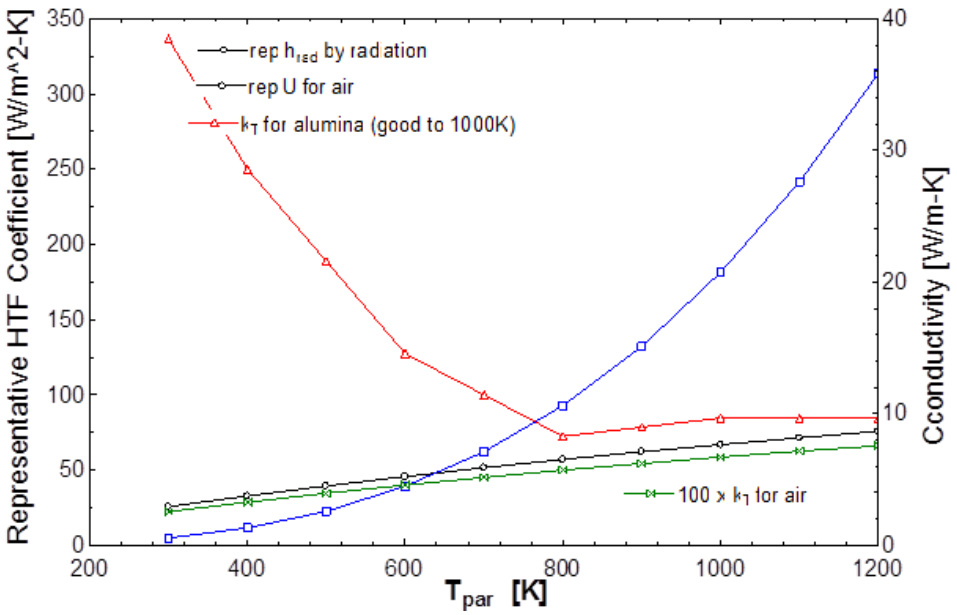

Figure 32 – Illustration of HPF bulk conductivity increasing with temperature

Therefore, the next step to improve this model is to incorporate a conductivity function depends on the temperature. Baumann et al. [18] have measured several particle conductivities at high temperatures using hot wire method, shown in Figure 33. While ID50 is mainly constructed with sintered bauxite particles with 300 μm in diameter, the conductivity function of sintered bauxite 0.6 (600 μm in diameter) is a reasonable approximation for that of ID50.

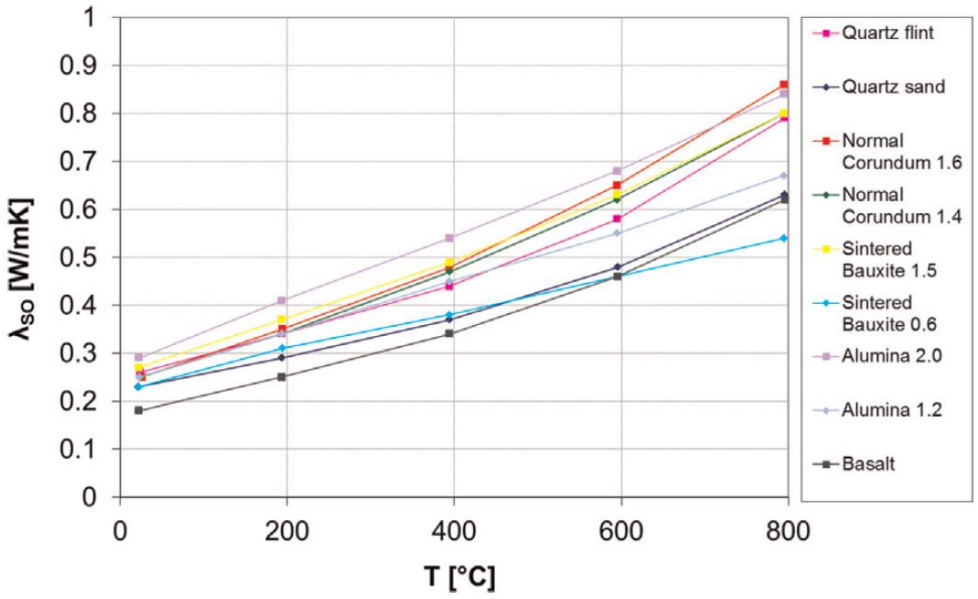

Figure 33 – Effective heat conductivity of various granular materials [18]

Since the correlation between the conductivity and temperature appears to be linear, a linear fit is applied, shown in Figure 34. Using this as the conductivity function, the simulated heat transfer coefficients increase from around 270 W/m^2-K to a range between 600 W/m^2-K and 700 W/m^2-K, shown in Figure 35. This large increment could be justified by the large increment in conductivity. From room temperature to the temperature range of 800 K to 1000 K, the conductivity increases from 0.220 W/m-K to about 0.475 W/m-K, which is more than twice of the conductivity at room temperature. Therefore, the heat transfer coefficient is expected to be larger than twice of its original value, which is proven by the simulation.

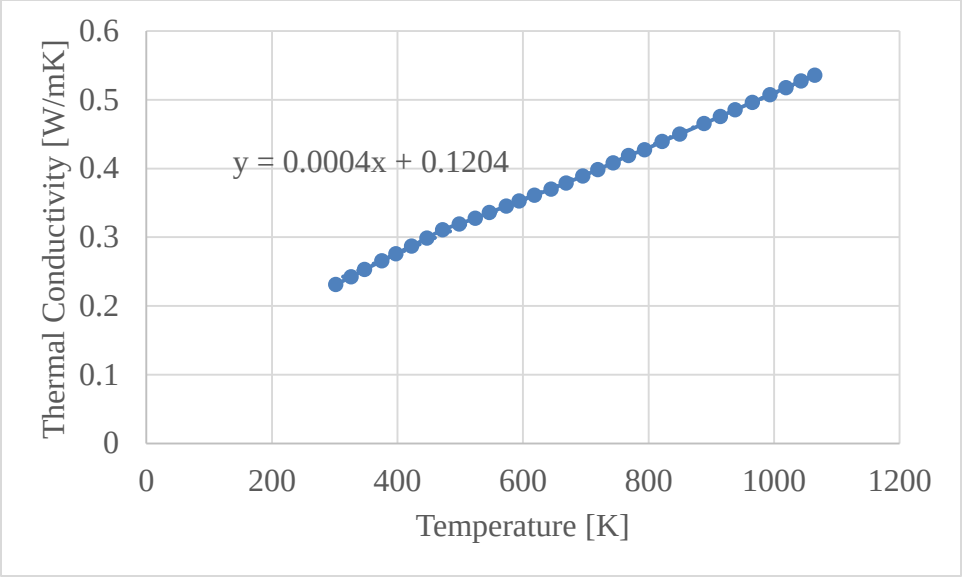

Figure 34 – Conductivity function

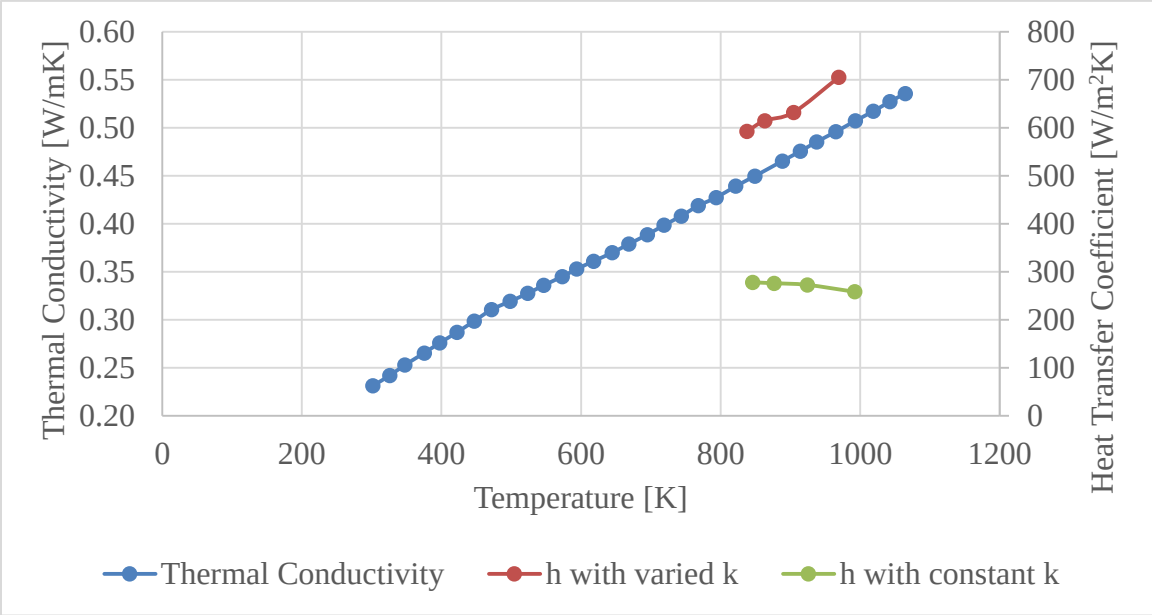

Figure 35 – Heat transfer coefficient comparison

4.6 Conclusion

The Euler-Euler laminar flow with continuous phase only has been proven to successfully model the particulate flow in heat exchanger. This modeling also simplifies a complicated 3D geometry into a 2D problem, using only one fluid to model a counter flow particulate heat exchanger. In addition, the bulk property of the HPF has been verified. Furthermore, due to the specify geometry of this heat exchanger, the near-wall thermal resistance is negligible.

This model has been tested and proven robust for change of geometry, change of geometry, change of inlet velocity and by taking thermal conductivity as a function of temperature. For future development, a 3D model using the same approach can be considered to incorporate particulate heat exchanger with fins or extended surface.

CHAPTER 5. FUTURE APPLICATIONS

5.1 Future Work for Approximate Euler HPF Model

The preceding analysis and modeling has shown that a numerically powerful Euler-Euler two phase flow model is adaptable to simulating an ultra-low viscosity single phase flow of a HPF that preserves the important kinematics of the plug flow observed in moving packed bed heat exchange processes. The ultra-low viscosity model, convergent for viscosity as low as 10^{-300} Pa-s, was also shown to perform much better than a more standard laminar flow model that was found to be convergent only for very low viscosities, around 10^{-10} Pa-s. With this approach, the HPF can be modeled with ultra-low viscosity, which is much lower than the typical fluids modeled in engineering, and approximately inviscid. Importantly, this model is implemented in a standard CFD package which has the geometric modeling, meshing, user-defined functions, and other features necessary for useful engineering applications of this approach.

While the purposes of this thesis were served by completing and testing the HPF model it is worthwhile to note some of the immediate and longer range applications possible with this approach.

At present, most or nearly all wall to particulate heat transfer experiments have been conducted at near ambient temperature, while all of the most promising applications, especially in CSP, are at high temperatures. Therefore, one of the most pressing needs, which is addressed previously, is modeling the heat transfer processes and calculating the heat exchange rate directly or estimating the heat transfer coefficient at higher

temperatures. The HPF approach only requires a reformulation of the thermal conductivity as a function of temperature to account for the anticipated enhancement at elevated temperatures. After this adjustment, it will be possible to more realistically model particulate to fluid heat exchangers for CSP and similar high temperature service.

Moreover, the existing particle to fluid exchanger designs are typically executed assuming a known and fixed particle inlet velocity. In practice, it may be preferable to vary this velocity, and in design it is certainly desirable to consider the inlet velocity as a free design variable. Since the HPF has been shown to be adaptable to varying inlet velocity in Section 4.4, this capability would significantly advance the modeling and design of particle to fluid exchangers. Since data for various particulates over a range of speeds is scarce, this modeling should be accompanied by a renewed experimental effort such as the one initiated already at Georgia Tech [1].

5.2 MATLAB Heat Exchanger Network Model

At current stage, it is not necessary to incorporated the 2D HPF model into a 3D model of particle to fluid heat exchanger, because the 2D model results are already somewhat accurate and costs computationally lower, although some researchers take this approach using even more complicated models on the particulate side. Instead, it is anticipated that the results of the heat transfer analysis will be summarized in terms of heat transfer coefficients dependent on particulate type, velocity, temperature, and flow thickness. A 2-D particulate heat exchanger is modeled through the principle of heat transfer, dividing the particulate flow and cooling fluid into small segments, shown in Figure 36. Essentially this is a heat exchanger network model for a single heat exchanger.

In the example shown, three streams of cooling fluid cool through each bank in the counter direction to the flow of particles. However, the network model developed to support this research, as described in the appendix, is adaptable to any number of tubes in the passes and any number of particle side streams. At present, the model contemplates mixing after each pass in accordance with a design now being deployed, however, fully sinusoidal flow in separate tubes can also be considered.

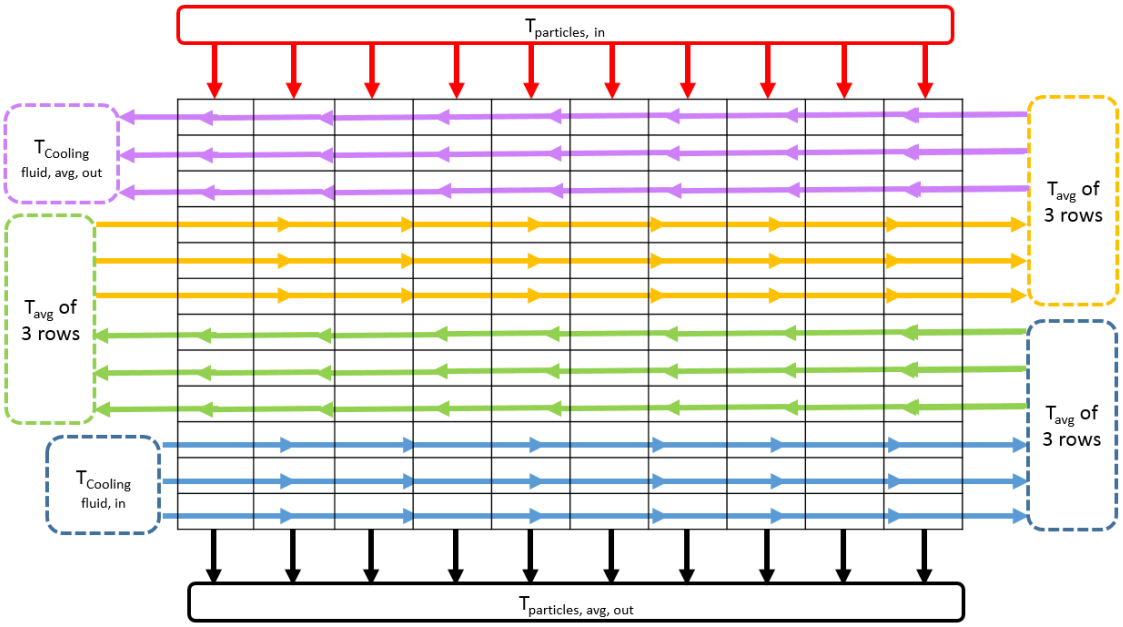

Figure 36 – Illustration of particle and cooling fluid flow

The heat transfer rate is calculated using the overall heat transfer coefficient, shown in Equation 18 and 19,

$$\dot{Q}_{RC} = (U_{overall}A)(T_{p,(R+1,C)} - T_{f,(R,C+1)}) \quad \text{for cooling stream from right to left} \qquad (18)$$

$$\dot{Q}_{RC} = (U_{overall}A)(T_{p,(R+1,C)} - T_{f,(R,C-1)}) \text{ for cooling stream from left to right} \quad (19)$$

where $\dot{Q}$ is heat transfer rate, $U_{overall}$ is overall heat transfer coefficient, A is heat transfer area, T is temperature. Subscript R is the row index, C is the column index, p represents the particle and f represents the cooling fluid. Presently two working fluids are under consideration, high pressure supercritical carbon dioxide (sCO_2) and moderate pressure air. Of course, low pressure air or liquid water for testing can easily be modeled as well. Currently this model is being tested and the results will be published elsewhere.

5.3 Other Designs of Particulate Heat Exchanger

Currently, every known particulate heat exchanger planned for near term service employ bare tubes or plates, and all are therefore only primary-surface exchangers without fins or other secondary surfaces. If the 2D HPF modeling approach in this thesis can be developed to a 3D model, it should be possible to model the performance of particle to fluid heat exchangers with extended surface and obtain reasonable simulation performance. Since some of the CSP applications in particular require operation a moderate to very high working fluid pressure, adding extended surfaces could be very economical, and the extended surfaces are not directly stressed by the fluid pressure. Indeed, fins or ribs might well be should to reinforce the primary tubing allowing for further economy. The application of extended surfaces is one promising method for reducing the cost of the particle to fluid heat exchanger, which is one of the most costly items hindering further CSP applications.

Very definitely results from this thesis can be applied to the improvement of the design for particle to fluid heat exchangers (PFHX) already proposed for CSP applications the extended modeling method can then be used to test different designs of particulate heat exchanger. For example, four particle-fluid heat exchanger designs [19] have been proposed as reasonable alternatives for CSP: (1) a serpentine finned-tube (SFT) design with plug flow on the particulate side, (2) a fluidized bed (FB) PFHX, (3) a design with thin or trickling particulate flow (with a free surface) called the zig-zag (ZZ) PFHX, and (4) a parallel pillow-plate (PP) PFHX also with plug flow. Most recently, use of finned tubing in the FB-FT-HX is also under consideration. The four general design concepts are illustrated in Figure 37.

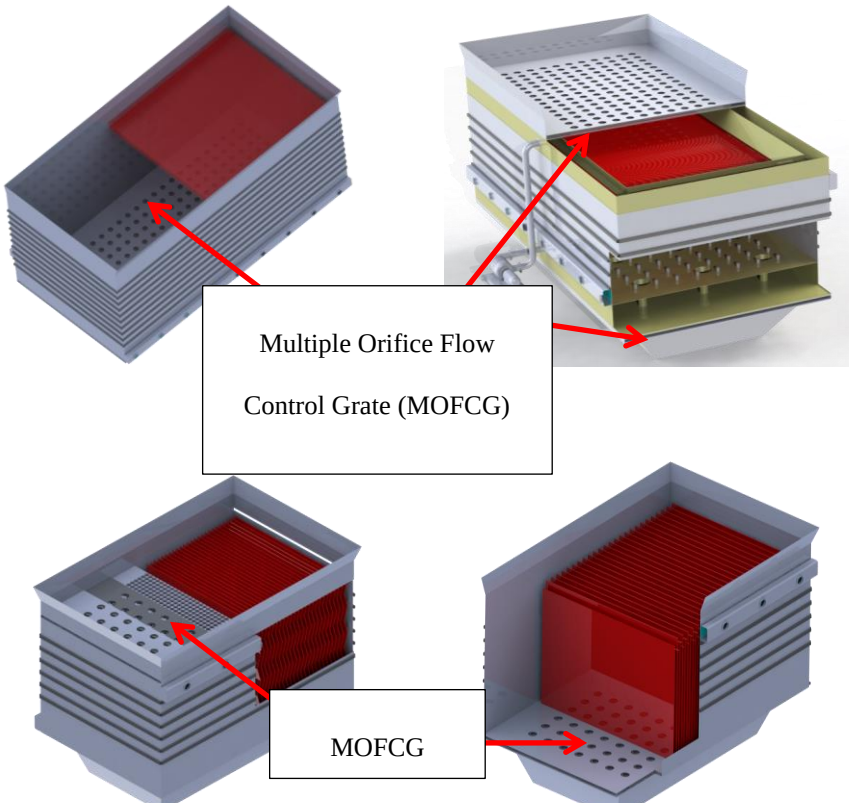

Figure 37 - Top Left: Serpentine Finned Tube (SFT) HX (most tubes omitted for clarity; Top Right: Fluidized Bed (FB) PFHX; Bottom Left: Zig-Zag (ZZ) trickling flow HX (corrugations exaggerated for clarity); Bottom Right: Parallel Pillow Plate (PP) HX (in section showing plates and MOFCG [18]

Methods from this thesis could be used to improve the modeling of the SFT PFHX by investigating and hopefully confirming the expected improved performance from using extended surfaces in such designs. Since this design is expected to be a multiple pass cross flow design, heat transfer coefficients obtained for various speeds and temperatures can be incorporated into the heat exchanger network model described in Section 5.2 above. A parametric study on particle inlet velocity could be performed for optimization to promote a higher heat transfer coefficient possible, as the heat transfer coefficient depends on the particle velocity. In addition, evaluation of the temperature enhancement of the heat transfer and the effectiveness of the fins based on analysis with the HPF can be used to improve the performance estimates.

The moving packed bed PP HX and the millimeter scale PP HX design can benefit from improved HPF analysis as discussed above. Another obvious application is optimizing the spacing in the PP-PFHX. But more importantly, a millimeter fluid-side diameter parallel plate exchanger, which is compatible with high pressure operation, is now under consideration. Such a design can be modeled by the HPF method for various particulate side velocities and plate spacing. A counterflow configuration is optimal for this application and this can be modeled by and extension of the techniques in this thesis, or a multiple pass design may be preferred for manufacturing considerations. The network heat exchanger model described in Section 5.2 can be used in this application.

It may be possible to extend the HFP approach to a rapid flow with free surface as needed for the proposed ZZ design. Despite the fact that a ZZ HX can use only half the exposed surface effectively the high heat transfer coefficient without the cost of fluidization could be helpful. In any event, the neat heat exchanger model developed for

this research can be usefully applied to this potentially high performance design, especially to help predict the higher temperature performance.

The previous designs are most likely to be compared with fluidized bed exchangers. The highly fluidized Circulating Fluidized Bed (CFB) concept was investigated [19], since this technology has great potential in particulate side heat transfer coefficient. However, CFB technology is probably not appropriate for particle heating receiver systems with thermal energy storage because the resulting particulate bed approaches uniform well-mixing. Since a uniformly mixed bed must be at the exit particulate temperature, the temperature-heat duty profile is very disadvantageous, resulting in extreme exergy destruction and making it impossible to achieve an exit working fluid temperature approaching the required temperature (650 °C) in a single stage HX.

In studying the FB approach, the prediction between heat transfer model and reported experimental results have a considerable disagreement. Amritkar and Tafti presented at a recent DOE workshop [20] showed heat transfer coefficient ranging from 300 to 500 and even to 900 W/m^2K for particles in the proposed size. Yet Zabrodsky [21] suggested a heat transfer coefficient range of 400 to 600 W/m^2K for particles; Fortunately, a fairly recent paper by Kim et al. [22] confirms the reasonably the well-regarded FB model by Zabrodsky [21]. Therefore, the more conservative heat transfer coefficient stated by Zabrodsky [21] can be considered in the modeling. This modeling can be enhanced by using the network model especially when sinusoidal tubes are considered. This network analysis can then be applied to evaluate potential FB exchangers, which can be compared with moving fixed bed and other exchangers.

Overall then it is shown that the methods developed, tested, and confirmed by comparison with experimental results have many applications in heat transfer theory and practice. In summary, this thesis research has successfully developed an equivalent CFD model to represent the flow and heat transfer processes in a moving packed bed heat exchanger. Furthermore some promising applications have been identified.

APPENDIX A. TYPICAL COMSOL INPUTS

Name	Expression	Value	Description
xP	0.114[m]	0.114 m	box x
zP	0.114[m]	0.114 m	box z
Dout	(5/8)[in]	0.015875 m	tube outer diameter
pitch	0.02 [m]	0.02 m	
Dheight	2.5[in]	0.0635 m	
Tin	(25+273.15)[K]	298.15 K	
Uin	0.01[m/s]	0.01 m/s	
Tairin	(484+273.15)[K]	757.15 K	
Tref	298.15[K]	298.15 K	
deltaT	48[K]	48 K	
qin	100[W/m^2]	100 W/m^2	
nu	15.11*10^-6 [m^2/s]	1.511E-5 m^2/s	

Figure 38 – Typical COMSOL Parameter Setting

	Property	Name	Value	Unit	Property group
☑	Dynamic viscosity	mu	1.81e-5[Pa*s]	Pa·s	Basic
☑	Ratio of specific heats	gamma	1.4	1	Basic
☑	Heat capacity at constant pressure	Cp	1.005[kJ/kg/...	J/(kg·K)	Basic
☑	Density	rho	1.205[kg/m...	kg/m^3	Basic
☑	Thermal conductivity	k	0.0257[W/m...	W/(m·K)	Basic
	Relative permeability	mur	1	1	Basic
	Relative permittivity	epsilonr	1	1	Basic
	Electrical conductivity	sigma	0[S/m]	S/m	Basic
	Speed of sound	c	cs(T[1/K])[...	m/s	Basic
	Refractive index, real part	n	1	1	Refractive index
	Refractive index, imaginary part	ki	0	1	Refractive index

Figure 39 – Air with constant properties at room temperature

APPENDIX B. MATLAB CODE

B.1 MATLAB Code for Network Model

```
clear all
close all
clc

Nrows = 12;
Ncols = 10;
N_per_row = 3;
UA = 30;
NC = Nrows * Ncols;
UA_C = UA/Nrows/Ncols;
C_P_Tot = 10;
C_F_tot = C_P_Tot;
C_dot_f = C_F_tot/N_per_row;
C_dot_p = C_P_Tot/Ncols;
NTU_F = UA/C_F_tot;
T_p_in = 100;
T_F_in = 0;
Q_dot_lim = C_P_Tot*(T_p_in-T_F_in);

MUX = 1;
C_R= MUX*C_dot_p/C_F_tot;
NTU_P = UA_C/C_dot_p;
eff_XF = 1-exp((NTU_P^0.22/C_R)*(exp(-C_R*NTU_P^0.78)-1));
EFF_C_min = eff_XF*C_dot_p;
eff_CF = (1-exp(-NTU_P*(1-C_R)))/(1-C_R*exp(-NTU_P*(1-C_R)));
eff_CF_BF = NTU_P/(1+NTU_P);
eff_HX_CT=1-exp(-NTU_P);

ParticleTemp = 100*ones(Nrows+1,Ncols);
FluidTemp = 100*ones(Nrows+1,Ncols+2);
HeatRatePerCell = ones(Nrows,Ncols);
compare = ones(Nrows+1,Ncols);

i = max( max(ParticleTemp-compare));

left = fliplr([1,2,3,7,8,9]);
right = [4,5,6,10,11,12];

while i > 10^-13
    ParticleTemp(1,:)= T_p_in;
    FluidTemp(1,:)= T_p_in;
    FluidTemp(11:13,1) = 0;
    FluidTemp(5:7,1) = mean(FluidTemp(8:10,2));
    FluidTemp(2,1) = mean(FluidTemp(2:4,2));
    FluidTemp(8:10,12) = mean(FluidTemp(11:13,11));
    FluidTemp(2:4,12) = mean(FluidTemp(5:7,11));
```

```
    for k = 2:Ncols+1
        for j = left+1
            FluidTemp(j,k)= FluidTemp(j,k+1)+HeatRatePerCell(j-1,k-
1)/C_dot_f;
        end

        for j = right +1
            FluidTemp(j,k)= FluidTemp(j,k-1)+HeatRatePerCell(j-1,k-
1)/C_dot_f;
        end
    end

    for k = 1:Ncols
        for j = left
            HeatRatePerCell(j,k) = EFF_C_min*(ParticleTemp(j,k)-
FluidTemp(j+1,k+2));
        end

        for j = right
            HeatRatePerCell(j,k) = EFF_C_min*(ParticleTemp(j,k)-
FluidTemp(j+1,k+1));
        end
    end

    for j = 2: Nrows+1
        for k = 1:Ncols
        ParticleTemp(j,k)= ParticleTemp(j-1,k)-HeatRatePerCell(j-
1,k)/C_dot_p;
        end
    end
    i = max( max(ParticleTemp-compare));
    compare = ParticleTemp;
end

T_P_avg = mean(ParticleTemp(end,:))
T_p_out = T_P_avg
T_F_out = FluidTemp(2,1)
Q_dot_tot = sum(sum(HeatRatePerCell))
Q_dot_P = C_P_Tot*(T_p_in-T_p_out)
Q_dot_F = C_F_tot *(T_F_out-T_F_in)
eff_HX = Q_dot_P/Q_dot_lim
eff_CFHX = NTU_F/(1+NTU_F)
LMTD = T_p_in - T_F_out
F_G = Q_dot_P /UA/LMTD
```

B.2 MATLAB Results Compared with Excel Model

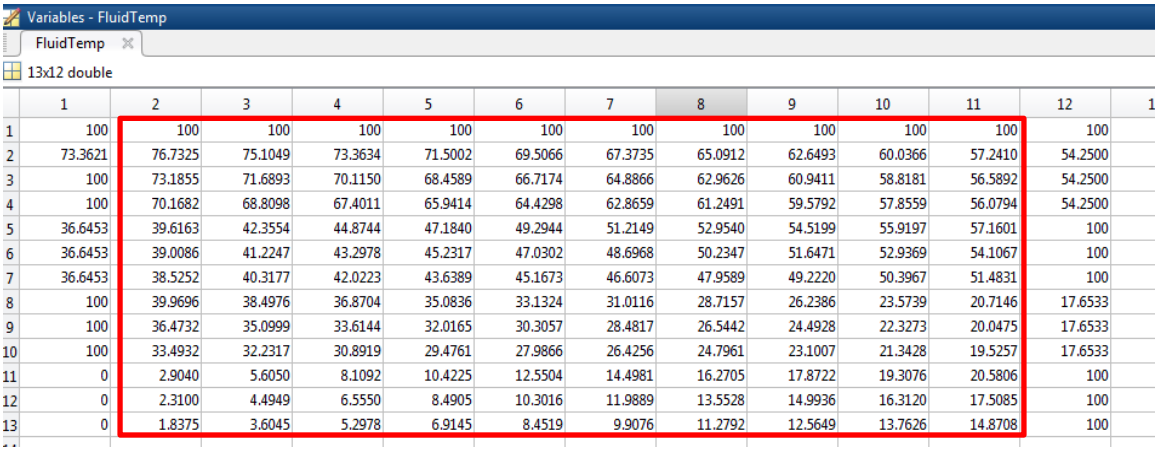

Variables - FluidTemp

FluidTemp

13x12 double

	1	2	3	4	5	6	7	8	9	10	11	12	1
1	100	100	100	100	100	100	100	100	100	100	100	100	
2	73.3621	76.7325	75.1049	73.3634	71.5002	69.5066	67.3735	65.0912	62.6493	60.0366	57.2410	54.2500	
3	100	73.1855	71.6893	70.1150	68.4589	66.7174	64.8866	62.9626	60.9411	58.8181	56.5892	54.2500	
4	100	70.1682	68.8098	67.4011	65.9414	64.4298	62.8659	61.2491	59.5792	57.8559	56.0794	54.2500	
5	36.6453	39.6163	42.3554	44.8744	47.1840	49.2944	51.2149	52.9540	54.5199	55.9197	57.1601	100	
6	36.6453	39.0086	41.2247	43.2978	45.2317	47.0302	48.6968	50.2347	51.6471	52.9369	54.1067	100	
7	36.6453	38.5252	40.3177	42.0223	43.6389	45.1673	46.6073	47.9589	49.2220	50.3967	51.4831	100	
8	100	39.9696	38.4976	36.8704	35.0836	33.1324	31.0116	28.7157	26.2386	23.5739	20.7146	17.6533	
9	100	36.4732	35.0999	33.6144	32.0165	30.3057	28.4817	26.5442	24.4928	22.3273	20.0475	17.6533	
10	100	33.4932	32.2317	30.8919	29.4761	27.9866	26.4256	24.7961	23.1007	21.3428	19.5257	17.6533	
11	0	2.9040	5.6050	8.1092	10.4225	12.5504	14.4981	16.2705	17.8722	19.3076	20.5806	100	
12	0	2.3100	4.4949	6.5550	8.4905	10.3016	11.9889	13.5528	14.9936	16.3120	17.5085	100	
13	0	1.8375	3.6045	5.2978	6.9145	8.4519	9.9076	11.2792	12.5649	13.7626	14.8708	100	

Figure 40 – Fluid Temperature Results from MATLAB

			Fluid Temp:										
			1	2	3	4	5	6	7	8	9	10	
	0		100.00	100.00	100.00	100.00	100.00	100.00	100.00	100.00	100.00	100.00	
"<-----	1	73.98	77.28	75.69	73.99	72.17	70.22	68.14	65.91	63.52	60.97	58.24	55.32
"<-----	2		73.81	72.35	70.81	69.20	67.49	65.71	63.83	61.85	59.78	57.60	55.32
"<-----	3		70.86	69.54	68.16	66.74	65.26	63.73	62.15	60.52	58.84	57.10	55.32
"----->	4	36.95	40.12	43.03	45.69	48.13	50.34	52.35	54.16	55.78	57.22	58.50	
"----->	5	36.95	39.43	41.75	43.92	45.94	47.81	49.55	51.14	52.61	53.95	55.16	
"----->	6	36.95	38.89	40.74	42.50	44.17	45.75	47.24	48.65	49.96	51.17	52.30	
"<-----	7		40.18	38.79	37.23	35.51	33.62	31.56	29.32	26.90	24.28	21.46	18.44
"<-----	8		36.78	35.48	34.05	32.51	30.85	29.08	27.19	25.18	23.05	20.80	18.44
"<-----	9		33.88	32.68	31.39	30.02	28.58	27.06	25.47	23.81	22.08	20.29	18.44
"----->	10	0.00	3.08	5.94	8.58	11.02	13.26	15.30	17.16	18.83	20.32	21.65	
"----->	11	0.00	2.41	4.69	6.84	8.86	10.75	12.51	14.14	15.65	17.03	18.28	
"----->	12	0.00	1.88	3.70	5.45	7.12	8.71	10.22	11.65	12.99	14.24	15.40	

Figure 41 – Fluid Temperature Results from Simple Excel Model

FluidTemp | HeatRatePerCell | ParticleTemp

13x10 double

	1	2	3	4	5	6	7	8	9	10
1	100	100	100	100	100	100	100	100	100	100
2	94.5747	94.1952	93.7891	93.3546	92.8898	92.3924	91.8602	91.2909	90.6816	90.0298
3	89.5873	88.9474	88.2690	87.5497	86.7871	85.9788	85.1221	84.2141	83.2520	82.2324
4	85.0593	84.2519	83.4032	82.5112	81.5740	80.5895	79.5556	78.4700	77.3303	76.1342
5	75.1560	75.1215	75.0067	74.8124	74.5394	74.1880	73.7584	73.2506	72.6643	71.9993
6	67.2785	67.7344	68.0964	68.3660	68.5444	68.6328	68.6319	68.5426	68.3652	68.1000
7	61.0124	61.7596	62.4142	62.9773	63.4499	63.8328	64.1267	64.3321	64.4494	64.4787
8	56.1058	56.3355	56.4581	56.4732	56.3807	56.1798	55.8698	55.4498	54.9183	54.2741
9	51.5280	51.3840	51.1316	50.7706	50.3007	49.7214	49.0319	48.2315	47.3190	46.2934
10	47.3228	46.9182	46.4122	45.8053	45.0977	44.2895	43.3808	42.3717	41.2621	40.0520
11	37.6427	37.9149	38.0649	38.0944	38.0047	37.7971	37.4727	37.0326	36.4776	35.8086
12	29.9427	30.6318	31.1981	31.6429	31.9674	32.1728	32.2599	32.2297	32.0830	31.8205
13	23.8178	24.7418	25.5537	26.2539	26.8428	27.3206	27.6876	27.9442	28.0905	28.1267

Figure 42 – Particle Temperature Results from MATLAB

	Particle Temp:										
	0	1	2	3	4	5	6	7	8	9	10
0		100.00	100.00	100.00	100.00	100.00	100.00	100.00	100.00	100.00	100.00
1		94.70	94.33	93.93	93.51	93.06	92.57	92.05	91.49	90.90	90.26
2		89.83	89.21	88.54	87.84	87.10	86.31	85.47	84.58	83.64	82.65
3		85.41	84.62	83.79	82.92	82.00	81.04	80.03	78.97	77.86	76.69
4		74.85	74.92	74.91	74.81	74.62	74.35	74.00	73.56	73.05	72.45
5		66.59	67.19	67.68	68.07	68.37	68.57	68.67	68.68	68.59	68.42
6		60.13	61.02	61.81	62.50	63.10	63.60	64.00	64.31	64.53	64.66
7		55.48	55.84	56.08	56.21	56.22	56.13	55.91	55.59	55.15	54.59
8		51.12	51.09	50.94	50.68	50.31	49.82	49.22	48.50	47.66	46.71
9		47.10	46.80	46.38	45.87	45.24	44.51	43.68	42.74	41.70	40.55
10		36.84	37.27	37.57	37.74	37.78	37.70	37.49	37.16	36.71	36.14
11		28.81	29.67	30.40	31.01	31.48	31.83	32.05	32.15	32.12	31.98
12		22.53	23.62	24.58	25.44	26.17	26.79	27.29	27.68	27.95	28.11

Figure 43 – Particle Temperature Results from Simple Excel Model

Variables - HeatRatePerCell

FluidTemp | HeatRatePerCell

12x10 double

	1	2	3	4	5	6	7	8	9	10	11
1	5.4253	5.8048	6.2109	6.6454	7.1102	7.6076	8.1398	8.7091	9.3184	9.9702	
2	4.9874	5.2477	5.5201	5.8050	6.1027	6.4136	6.7381	7.0767	7.4297	7.7974	
3	4.5280	4.6955	4.8658	5.0384	5.2131	5.3893	5.5665	5.7442	5.9216	6.0981	
4	9.9033	9.1304	8.3965	7.6988	7.0346	6.4016	5.7972	5.2194	4.6660	4.1350	
5	7.8775	7.3870	6.9102	6.4465	5.9950	5.5552	5.1265	4.7080	4.2992	3.8993	
6	6.2661	5.9749	5.6823	5.3887	5.0945	4.8000	4.5052	4.2105	3.9158	3.6213	
7	4.9066	5.4240	5.9561	6.5040	7.0692	7.6530	8.2569	8.8823	9.5310	10.2046	
8	4.5778	4.9516	5.3265	5.7026	6.0800	6.4584	6.8379	7.2183	7.5993	7.9807	
9	4.2052	4.4658	4.7193	4.9653	5.2030	5.4319	5.6511	5.8598	6.0569	6.2415	
10	9.6801	9.0033	8.3473	7.7109	7.0930	6.4924	5.9081	5.3391	4.7845	4.2434	
11	7.7000	7.2831	6.8669	6.4515	6.0373	5.6243	5.2128	4.8029	4.3946	3.9881	
12	6.1249	5.8900	5.6444	5.3890	5.1247	4.8522	4.5723	4.2855	3.9925	3.6938	
13											

Figure 44 – Heat rate per cell from MATLAB

		Heat Rate per Cell used above:										
	0		1	2	3	4	5	6	7	8	9	10	
"<-----	1		5.30	5.67	6.07	6.49	6.94	7.43	7.95	8.51	9.10	9.74	55.32
"<-----	2		4.87	5.13	5.39	5.67	5.96	6.26	6.58	6.91	7.26	7.62	55.32
"<-----	3		4.42	4.59	4.75	4.92	5.09	5.26	5.44	5.61	5.78	5.96	55.32
"----->	4		10.56	9.70	8.88	8.11	7.38	6.69	6.03	5.41	4.81	4.24	
"----->	5		8.26	7.74	7.23	6.73	6.25	5.78	5.33	4.89	4.45	4.03	
"----->	6		6.46	6.17	5.87	5.57	5.27	4.97	4.67	4.37	4.06	3.76	
"<-----	7		4.65	5.18	5.73	6.29	6.87	7.47	8.09	8.72	9.39	10.07	18.44
"<-----	8		4.36	4.75	5.14	5.53	5.92	6.31	6.70	7.09	7.48	7.88	18.44
"<-----	9		4.02	4.29	4.56	4.82	5.07	5.31	5.54	5.76	5.97	6.16	18.44
"----->	10		10.26	9.53	8.81	8.13	7.46	6.81	6.18	5.58	4.98	4.41	
"----->	11		8.03	7.60	7.17	6.73	6.30	5.87	5.44	5.02	4.59	4.17	
"----->	12		6.28	6.06	5.82	5.57	5.31	5.04	4.76	4.47	4.17	3.87	

Figure 45 – Heat rate per cell from Simple Excel Model

Table 11 – Key values comparison

Item	MATLAB Result	Excel Result
$T_{particle,out}$	26.64	26.02
$T_{fluid,out}$	73.36	73.98
$\dot{Q}_{particle}$	733.62	739.84
$\dot{Q}_{fluid}$	733.62	739.84
eff_{HX}	0.73	0.74
eff_{CFHX}	0.75	0.75
LMTD	26.64	26.02

REFERENCES

1. Nguyen, C.M., *Heat transfer coefficients of particulate in tubular heat exchangers.* (Master's thesis), Georgia Tech Theses and Dissertations, 2015.

2. *COMSOL Multiphysics® 5.2*. 2016, COMSOL, Inc. : Burlington, MA, USA.

3. National Renewable Energy Laboratory (NREL), G.I.o.T.G.T., Babcock & Wilcox (B&W), Solex Thermal, Vacuum Process Engineering (VPE), *High-Temperature Particle Heat Exchanger for sCO2 Power Cycles Phase 1 Continuation Report.* 2016.

4. *Which Multiphase Flow Interface Should I Use?* 2015 [cited 2017; Available from: https://www.comsol.com/blogs/which-multiphase-flow-interface-should-i-use/.

5. Theodore L. Bergman, A.S.L., Frank P. Incropera, David P. DeWitt, *Fundamentals of Heat and Mass Transfer*. 7th ed. 2011: Wiley.

6. Cess, R.D. and E.C. Shaffer, *Heat transfer to laminar flow between parallel plates with a prescribed wall heat flux.* Applied Scientific Research, Section A, 1959. **8**(1): p. 339-344.

7. Shah, R.K. and M. Bhatti, *Laminar convective heat transfer in ducts.* Handbook of single-phase convective heat transfer, 1987. **3**.

8. Sparrow, E., J. Novotny, and S. Lin, *Laminar flow of a heat‐generating fluid in a parallel‐plate channel.* AIChE Journal, 1963. **9**(6): p. 797-804.

9. Pohorecki, R., J. Bridgwater, and M.M.R.G.C. Gallegos, *Chemical Engineering and Chemical Process Technology - Volume I: Fundamentals of Chemical Engineering*. 2010.

10. Kevin J. Albrecht, C.K.H., *HEAT TRANSFER MODELS OF MOVING PACKED-BED PARTICLE-TO-SCO2 HEAT EXCHANGERS.* Proceedings of the ASME 2017 Power and Energy Conference, 2017.

11. *KD2 PRO*. 2015 [cited 2017; Available from: https://www.decagon.com/en/thermal/instruments/kd2-pro/.

12. Ho, C.K., *High Temperature Falling Particle Reciver*. 2013.

13. *Sphere packing*. [cited 2017; Available from: https://commons.wikimedia.org/wiki/File%3AClose_packing_box.svg.

14. Martinek, J. and Z. Ma, *Granular Flow and Heat Transfer Study in a Near-Blackbody Enclosed Particle Receiver.* 2014(45868): p. V001T02A012.

15. Patil, D.J., et al., *Wall-to-bed heat transfer in gas–solid bubbling fluidized beds.* AIChE Journal, 2006. **52**(1): p. 58-74.

16. Ho, C.K., *High-Temperature Particle Heat Exchanger for sCO2 Power Cycles Presentation*. 2016.

17. Honda, R., H. Umekawa, and M. Ozawa, *Heat transfer and flow characteristics around a finned-tube bank heat exchanger in fluidized bed.* Nuclear Instruments and Methods in Physics Research Section A: Accelerators, Spectrometers, Detectors and Associated Equipment, 2009. **605**(1): p. 188-191.

18. Baumann, T. and S. Zunft, *Properties of granular materials as heat transfer and storage medium in CSP application.* Solar Energy Materials and Solar Cells, 2015. **143**: p. 38-47.

19. Center, S.N.L.G.I.o.T.B.U.K.S.U.G.A., *High Temperature Falling Particle Receiver*. 2014.

20. Amritkar, A. and D. Tafti, *Heat Transfer in Fluidized Bed-Tube Heat Exchanger*, in *NETL Workshop on Multiphase Flow Science*. 2013.

21. Zabrodsky, S.S., *Hydrodynamics and heat transfer in fluidized beds*. 1963: MIT Press.

22. Kim, S.W., International Journal of Heat and Mass Transfer, 2003. **46**: p. 399 - 409.